Rivalry in Sibling *Bacillus subtilis* Colonies: Enemy or Family?

by

Rajorshi Paul

A thesis submitted in partial fulfilment of the requirements for the degree of

Master of Science

Department of Mechanical Engineering

University of Alberta

© *Rajorshi Paul*, 2019

Abstract

A bacterial colony constitutes a complex microcosm which is equipped with a wide range of defensive adaptations that allow the colony to survive adverse environmental conditions and predation. The extreme resilience of bacteria in colonies has been a subject of continued research for nearly two centuries. Although many aspects of bacterial dynamics have been well studied, several features of bacterial growth and dispersion inside colonies remain unexplored. In this thesis, I present my research on the interaction between two bacterial colonies. When two bacterial colonies interact with each other the interaction may be mutually beneficial or inhibitory in nature. It has been found that two *Bacillus subtilis* colonies growing adjacent to each other on a nutrient rich agar plate exhibit two distinct types of interactions: they either coalesce as they grow or form a distinct interface at the colony fronts without complete coalescence. The nature of interaction depends on the agar concentration in the growth medium and the initial separation between the colonies. When the agar concentration was lower than 1%, two sibling colonies were found to coalesce. At 1% or higher concentrations, colonies formed an interface when the separation between the colonies was 20 mm or higher. Interactions of a colony with solid structures and liquid drops have indicated that biochemical rather than presence of physical barriers are responsible for the interface formation. Based on the experimental findings, a reaction diffusion model has been formulated to numerically simulate the two interaction patterns. The model predicts if two sibling colonies will form an interface under the given combination of agar concentration and separation between the colonies. The model prediction agrees well with experimental findings and generates a dimensionless phase diagram containing coalescence and separation domains. The dimensionless critical separation $\overline{d}^*$ which demarcates the two interaction regimes was found to follow a simple power law in terms of the ratio of the diffusion coefficients $\overline{D}$ of the colony to the nutrients : $\overline{d}^* = \alpha \overline{D}^n$.

Preface

The research presented in this thesis has resulted in a scientific article, titled "Rivalry in Sibling *Bacillus subtilis* Colonies: Enemy or Family?" which has been submitted for publication. I have been responsible for literature review, data analysis and manuscript writing. Dr. Tanushree Ghosh has assisted me in performing some of the experiments. Dr. Tian Tang and Dr. Aloke Kumar have been supervisory co-authors. This thesis is presented in a monograph format.

Acknowledgements

When I began my Master's degree program in January, 2017, I was quite apprehensive having to start a life in a foreign country away from my family, nearly halfway across the globe. Fast forward two years, I am on the verge of wrapping up my research. The journey has been smooth sailing and all the credit goes to my supervisors, course instructors, and the rich network of colleagues and friends that I cultivated during this period. I am grateful to everyone who contributed to my thesis, either directly or indirectly through their guidance, mentorship and warm camaraderie.

I am indebted to my graduate supervisors Dr. Tian Tang and Dr. Aloke Kumar for their invaluable advice, encouragement and teaching me the finer skills associated with graduate research, specifically the art of presenting technical content in research presentation, article and poster formats. Weekly individual meetings with my supervisors have undeniably changed my perception of scientific research and pushed me towards a timely completion of my graduate research. I am also very grateful to Dr. Tanushree Ghosh, with whom I have had the pleasure of working closely, learning about the experimental techniques in bacteriological studies required for my study. Without Dr. Ghosh's assistance in performing my experiments and her expertise in microbiology, it would perhaps not have been possible to complete my research.

I am sincerely grateful to Dr. Cagri Ayranci, and his students Irina Garces and Xiaoang Ma for promptly assisting me with characterizing agar gel samples on the compression testing rig in Dr. Ayranci's lab. I also thank Dr. Howard Ceri, University of Calgary for graciously providing us *Pseudomonas fluorescens* strains for my experiments. I am very grateful to the Faculty of Graduate Studies and Research (FGSR), and the Mechanical Engineering department especially Gail, Richard and Isabelle who were always there to help me out whenever I was faced with any academic or administrative problems.

I cannot begin to thank the funding agencies for sponsoring my research. I truly appreciate the Alberta Bio Future Research and Innovation Program, Alberta Innovates Bio Solutions, Government of Alberta, Canada for funding my Master's research. This research has been sponsored under the project title "Engineering lignin as a precursor for carbon fiber using novel biodegradation and purification techniques" (BFR032) headed by Dr. Tian Tang, Dr. Aloke Kumar and Dr. Cagri Ayranci. I am also thankful to Shell Canada for sponsoring my conference travels in 2017 and 2018 through the Shell Enhanced Learning Fund (SELF) program.

Last but not the least, I want to thank my colleagues at NINT, the members of the Kumar Biomicrofluidics lab and Dr. Tang's group, and the friends that I made in the course of two years. Times spent with them at work and outside of work have not only enriched me professionally but has had a deep impact on me at the personal level. Finally, I am grateful for the love, inspiration and constant encouragement of my family to whom this thesis is dedicated.

Table of Contents

List of Tables

List of Figures

Chapter 1
Introduction

Bacterial colonies are excellent examples of active soft matter, where individual cells interact with each other as well as the external environment through physical and biochemical stimuli [1-4]. Inside these colonies bacterial cells can interact with each other using mechanisms that operate over several different length and time scales [5], such as by means of intercellular signaling [6-11], such as quorum sensing [12-14] as well as by production of biofilms and other extracellular materials [15-17]. Intercellular coordination in a colony allows bacteria to swarm on agar plates to derive nutrition from growth medium [18-22], produce fruiting bodies and sporulation [23, 24], and ensure their survival against external threats and adverse environmental conditions [25-27]. Bacterial colonies are equipped with a myriad of intricate defense strategies to protect themselves from predators, compete for limited resources, and adapt and respond to outside stimuli [25, 28]. Interestingly, cues from the external environment can bring about measurable changes in the growth of bacterial colonies; changes in bacterial colonies due to such factors comprise an important domain of biophysical research [5].

When multiple bacterial colonies grow in close proximity, they interact with each other to compete for limited resources present in the growth medium. By means of biochemical sensing, bacteria can identify the neighbor colonies as enemy or family [1, 29-31], and this identification can affect their biophysical responses such as growth pattern, growth rates and the way they interact with the neighbor. Patra et al. and Chakraborty et al. reported the formation of an interface between two different species of bacteria interacting with each other on an agar plate [32, 33]. When colonies of the same species (i.e. sibling colonies) interact, one may observe either inhibition by cell death

forming an interface or complete coalescence. For instance, sibling colonies of identical strain of *Proteus mirabilis* coalesce when they interact but inhibition occurs between different strains of the *P. mirabilis* [29]. *Paenibacillus dendritiformis* has been found to form interfaces even between sibling colonies of identical strains [4]. Matsushita and coworkers reported that sibling *Bacillus subtilis* colonies exhibit both interaction patterns under different nutrient conditions: interfaces form on nutrient deficient agar plates [34], while coalescence occurs in nutrient rich environments [35].

The nature of interaction between two bacterial colonies may be governed by a number of biochemical and physical factors. Biochemical factors include the substrate which acts as the nutrient source, the species of bacteria taking part and the mutation in these species. These factors influence the growth of bacterial colonies and are, thereby, expected to affect their interactions. On the other hand, spreading of bacterial colonies has been found to be dictated by physical factors such as osmotic pressure [36-38], surface tension [15, 39-42], permeability and viscous drag of the growth medium [43]; these may be influenced by the concentration of agar and nutrients, and the bacterial strain used. To understand the dynamics of inter-colony interactions, it is necessary to study the role of these physical and biochemical factors. Studies on colony interactions by Be'er et al. [4, 28, 44, 45] and Chakraborty et al. [32] found that certain biochemical inhibition factors produced by the interacting colonies are responsible for cell death, leading to interface formation as a means of surviving the competition for limited resources. The investigation by Be'er et al. further showed that in *P. dendritiformis*, the concentration of agar and initial separation between inoculated colonies influence the front propagation of the sibling colonies [4], but the exact role of these physical factors were not studied in detail. Investigating the role of physical factors in the interaction of multiple bacterial colonies can be expected to yield insights into the spreading dynamics of bacterial soft matter. In fact, physical parameters such as agar concentration and colony separation can be

expected to impact bacterial colony dynamics, and yet an exhaustive understanding of the role of these factors remains largely unexplored.

To address these scientific lacunae, the influence of agar concentration and initial separation between two sibling *B. subtilis* colonies on the nature of interaction between them has been studied. *B. subtilis* is known to possess swimming and swarming motility which enable the bacteria to move quickly through semi-solid agar media [46]. Agar concentration controls the radial spreading of each colony whereas the initial separation between the colonies signifies their maturity when they start interacting. Systematic experiments are performed in nutrient-rich growth media by varying the agar concentration and initial colony separation. To complement the experimental study, a reaction-diffusion model is established to predict the interaction patterns: coalescence and interface formation. Good agreement between the mathematical model and experiments facilitates the generation of a phase diagram that quantitatively describes the coalescence and interface regimes of the *B. subtilis* colony interactions.

Chapter 2
Literature Review

2.1 Overview of Bacteria

Bacteria are one of the most primitive organisms on this planet. They are extremely resilient and are capable of surviving extreme environmental conditions. This has made bacteria a subject of extensive research for the past two centuries. First discovered by Antony Van Leeuwenhoek [47] in 1676, bacteria have been studied for their salubrious as well as pernicious effects on health. Today, bacteriological research finds applications in almost all walks of life including but not limited to medical sciences, food industry, and oil and gas industry.

Bacteria are unicellular organisms which may be rod shaped, spherical or even helical. Bacterial cells typically vary from 0.5 μm to 5 μm in size. Each bacterial cell consists of a cell wall which may be classified as Gram-positive as in *Bacillus subtilis*, or Gram negative, e.g., *Escherichia coli*. The cell wall encloses a cytoplasm where the bacterial DNA is present. Most bacteria contain certain extra-cellular structures of which the most important are the flagella. Flagella are the primary locomotory organelles in bacteria. These are long whip-like filaments extruding from the cell walls and attached to biological motors which cause the structures to rotate both in clockwise (CW) and counter clockwise (CCW) directions with angular velocities as high as 100,000 rpm [48]. The number and location of flagella on a bacterium varies with the species and the strain. Peritrichous bacteria such as *E. coli* and *B. subtilis* contain multiple flagella. Such bacteria are generally highly motile [49]. A typical bacterial cell is depicted in Figure 2.1.

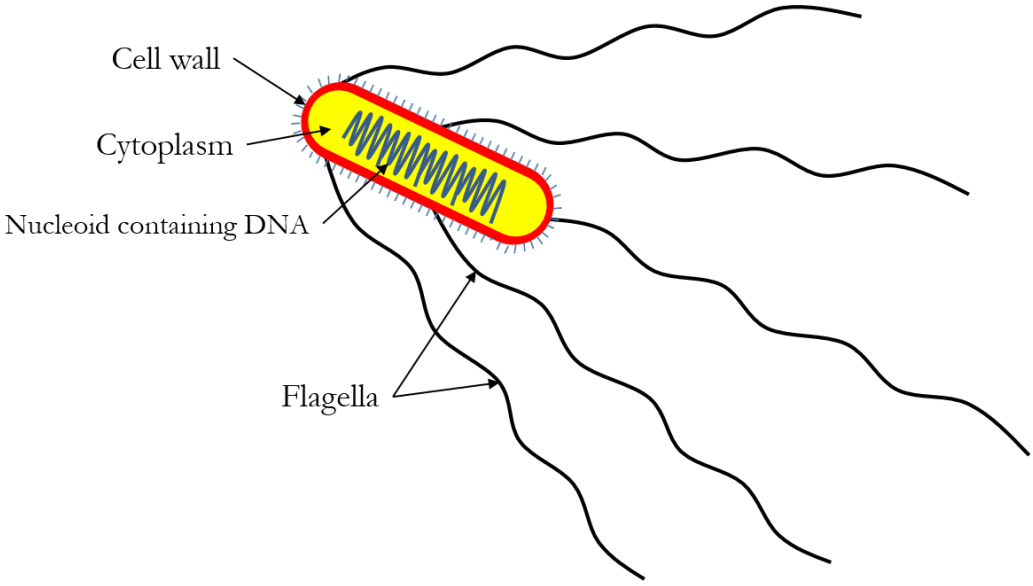

Fig. 2.1. A typical peritrichous bacterial cell showing important cell structures.

Flagella allow bacteria to execute three primary modes of locomotion:

- *Swimming*: Swimming is the flagellar motility causing translation of the bacterial cells through a liquid medium. It is brought about by synchronized rotation of the flagella in the same direction. In *E. coli*, the CCW rotation of the flagella helps the bacterium to generate thrust pushing the cell forward. The CCW rotation occurs intermittently which produces a translation in random directions. Swimming motility can produce speeds from 20 μm/s to as high as 60 μm/s [49].
- *Tumbling*: Tumbling motility is caused by the CW rotation of the flagella. This causes the bacteria to reorient rapidly. Therefore, tumbling motility produces a steering effect, which is not possible in swimming. Swimming and tumbling, in tandem, helps bacteria navigate through liquid media [49, 50] (see Figure 2.2).

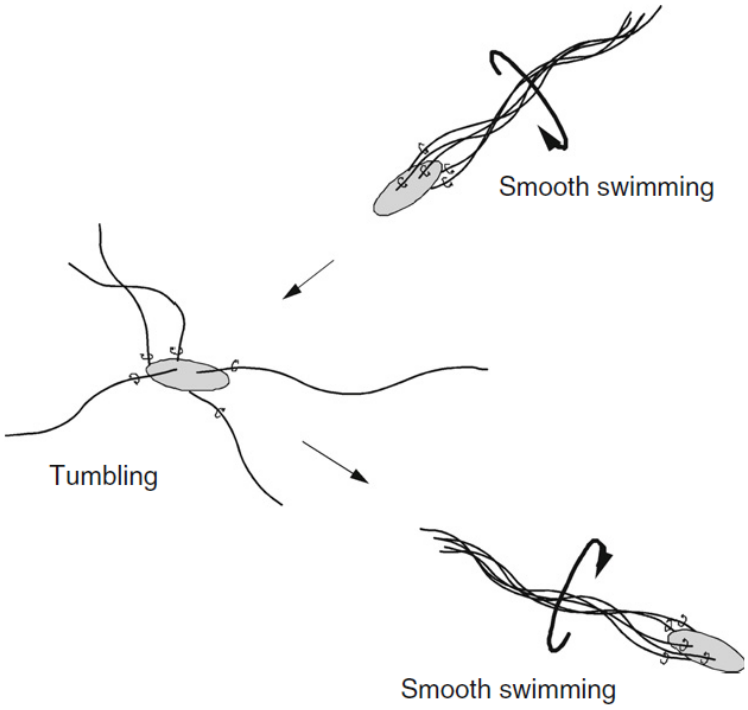

Fig. 2.2. Swimming and tumbling motilities help bacterial cells move forward and change directions in liquid media. Swimming occurs by CCW rotation of bundled flagella and tumbling occurs when flagella spread out and rotate in CW direction. Reprinted from *International review of cell and molecular biology* , Vol 270, H. Terashima, S. Kojima, M. Homma, "Flagellar motility in bacteria: structure and function of flagellar motor", pp 39-85, Copyright (2008), with permission from Elsevier.

- *Swarming*: Swarming is a rapid collective motion of bacterial cells on surfaces of semi-solid media which is brought about by flagellar rotation reaching speeds of the order of several centimeters per hour [19]. Swarming is often accompanied by production of biosurfactants, such as surfactin in *B. subtilis* [40]. Spreading of bacterial colonies on agar plates is brought about by swarming of bacteria on the surface of agar medium. It is to be noted that at very low agar concentrations, the pore size of the semi-solid medium is large enough so that bacteria can swim freely throughout the bulk medium. Only at high concentrations when the

pores are small that bacteria resort to coordinated swarming on the surface of the semi-solid medium [19, 51].

Movement of bacteria is caused by external stimuli such as presence of nutrients and biochemicals (chemotaxis), temperature (thermotaxis), light (phototaxis), gravity (gravitaxis) among others. Bacteria are equipped with different sensory systems [52-54] which allow them to detect any change in external environment and move accordingly to ensure its survival.

Bacterial cells proliferate by means of cell division and the rate at which the population grows is controlled by the external environment. Factors such as temperature, pH, and availability of nutrients control the rate of cell division. In adverse conditions, instead of dividing, certain bacteria collectively produce spores (usually in Gram-positive bacteria) and fruiting bodies which are resistant to harsh conditions [24, 55]. Under appropriate conditions of temperature, pH and nutrients, bacterial culture in a liquid medium exhibits four distinct stages of growth:

- *Lag phase*: In this phase, bacteria exhibit minimum activity and population growth is almost non-existent. During this phase, bacteria familiarize themselves with the environment and prepare for cell division.
- *Log phase*: In this phase, bacteria consume the available nutrients and grow in population. In this phase, bacteria are at their most active stage. Bacteria used in microbiological studies are generally procured when the culture is in the log phase.
- *Saturation phase*: As the bacteria continue to consume nutrients from the solution, the medium gradually gets nutrient depleted. In this stage, competition for the limited nutrients causes the bacterial population to stabilize to a saturation value. This stage is known as the saturation phase.

- *Death phase*: As the medium becomes severely depleted of nutrients, bacterial cells start dying. Consequently, after a long time post incubation, bacterial population declines. This is the death phase.

A schematic of a typical growth curve is shown in Figure 2.3.

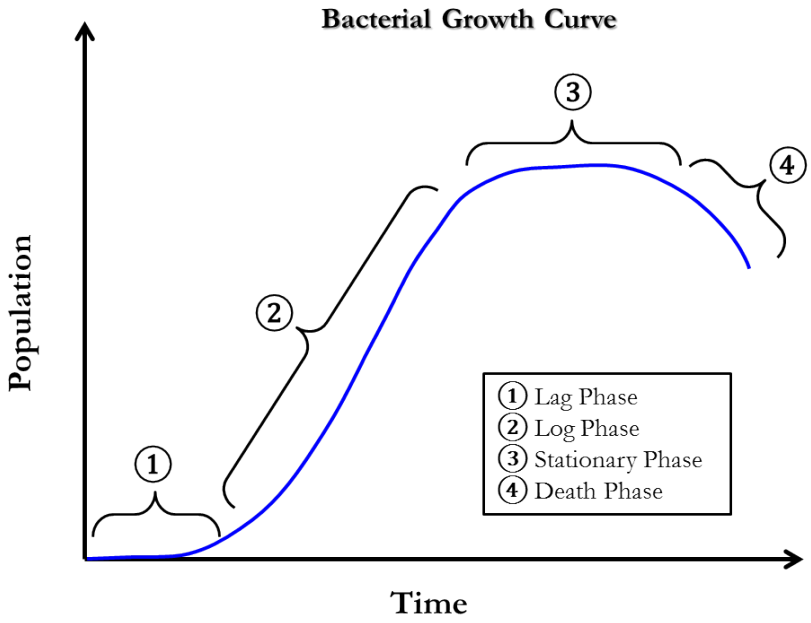

Fig. 2.3. A typical bacterial growth curve showing the four stages of growth.

Instead of a liquid medium, if bacteria are allowed to grow on semi-solid surfaces, colonies are formed. The semi-solid growth medium is generally prepared by heating a solution of agar and nutrients to prepare a hydrogel. Colonies are grown on the surfaces of these agar-based growth media. Within a colony, bacteria feed on nutrients and divide by binary fission and as the population grows, they spread out in different directions in search of nutrients, forming complex and diverse colony morphologies. Figure 2.4 shows the different colony morphologies observed in *B. subtilis* at different agar and nutrient concentrations.

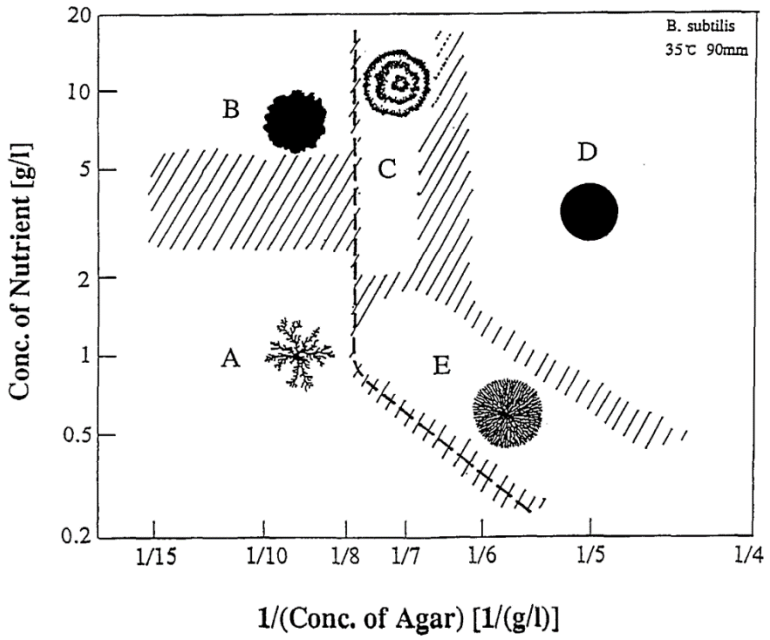

Fig. 2.4. *B. subtilis* exhibits different morphologies depending on the nutrient and agar concentrations in the growth medium. Image reproduced from [35] © (1994) the Physical Society of Japan.

As the colony matures, the individual cells produce an extracellular matrix which envelopes the colony. The spreading of colonies on agar plates is influenced by both biochemical and physical factors. The composition of the source of nutrients, the bacterial species as well as the mutations in the bacteria are some of the biochemical factors which affect the colony spreading and morphology. The nutrient source is generally composed of different components and the relative amount of each component may influence the characteristics of the colony. Each species of bacteria is unique in terms of their biochemical activities. For instance, production of surfactin by *B. subtilis* allows the colony to spread much faster than *E. coli* which does not produce biosurfactants. Again, certain mutations of *B. subtilis* which do not produce biosurfactants have different colony spreading characteristics compared to their counterparts which do [39]. Apart from biochemical factors, physical factors such as osmotic pressure [36-38], surface tension [15, 39-42, 56] as well as viscosity

and permeability of the growth medium [43] affect the spreading characteristics of colonies. Seminara et al. found that in *B. subtilis*, osmotic pressure imbalance between growth medium and colony created by nutrient uptake causes the extra-cellular matrix of the colony to expand, which drives colony spreading [36]. Friction between the cell bodies of the bacteria and the surface of the semi-solid growth media makes it difficult for bacteria to navigate the surface and derive nutrition. Certain bacteria secrete biosurfactants which increases surface wetting and promote swarming motility on agar surfaces, and thereby influences both colony spreading and morphology [15, 57]. Recently, Yang et al. found that in *Pseudomonas aeruginosa* colonies, reduced permeability of the growth medium has an adverse effect on the swarming motility. They also showed that by increasing the viscosity of the agar medium, the swarming motility of the bacteria reduces [43]. These physical factors are controlled by the concentrations of nutrient and agar in the growth medium [58]. Production of biosurfactants by certain bacteria alters the wetting properties of the colony and therefore, the species and the mutation of bacteria also influence the aforementioned physical factors [15, 39].

2.2 Multicellularity of Bacteria

Prior to 1970, it was commonly believed that bacteria, being unicellular, are asocial and individualistic in nature, unlike multicellular organisms. However, bacteria are known to execute complex activities such as distinguishing between different species and strains, execute coordinated locomotion. Such complex activities are characteristics of multicellular organisms, unlikely to be performed by a group of individual asocial cells [1]. In 1970, Nealson and co-workers found one of the first evidences to communications between bacterial cells [59]. For their study, they used *Vibrio fischeri*, a species of marine bacterium known to have bioluminescent properties. They performed two sets of experiments. In the first experiment, they grew *V. fischeri* in a standard liquid growth medium and found that *V. fischeri* produced strong bioluminescence when the density of cells in the

growth culture is higher than a critical value. Below this critical cell density, bioluminescence is negligible. In the second set of experiments, they grew the bacteria in a conditioned medium. To prepare the conditioned medium, Nealson and co-workers prepared a culture of a mutant strain of *V. fischeri* in a standard liquid growth medium up to a particular cell density. Then they removed the cells from the culture medium and sterilized the medium. This sterile culture medium was used in the second set of experiments as the conditioned medium. Interestingly, when *V. fischeri* cells were grown in the conditioned medium, they were able to induce luminescence at much lower cell densities [60]. The phenomenon of bioluminescence in *V. fischeri* is explained in terms of certain signalling biomolecules produced by cells of both strains of *V. fischeri*, known as "autoinducers". When the concentration of the autoinducers reaches a critical concentration, it triggers luminescence. This explains why luminescence occurs only when the density of the cells is high and is suppressed below a critical density in the first set of experiments. The conditioned medium used in the second set of experiments already contains autoinducers, secreted by the mutant strain of *V. fischeri*. Hence, when the bacteria are grown in the conditioned medium, luminescence is observed even at a low density of *V. fischeri*. The experiments of Nealson and co-workers demonstrated that bacteria communicate with each other by means of biochemical signals. This type of primitive biochemical communication is broadly termed as "quorum sensing" [10, 12-14, 61, 62]. Bacterial cells produce a wide range of biomolecules as chemical signals which activate receptors on bacteria. These receptors are extremely specific and can be activated only by certain molecules. Intercellular signalling by means of quorum sensing renders multicellularity in bacteria allowing them to exhibit high degrees of coordination with each other inside colonies. Intercellular signalling and multicellularity are essential for the survival of bacterial colonies and are manifested in the form of kin recognition [31, 63-65], swarming motility [19, 30, 57], chemotaxis to derive nutrition, spore and fruiting body formation [23, 55], biofilm formation [66], biosurfactant production [15, 67] as well as

interaction with the external environment to survive predation and adverse environmental conditions .

2.3 Interactions Between Bacterial Colonies

Biochemical signals generated by bacteria are unique to the species as well as the strain of the bacteria. This allows the bacteria to distinguish between identical and alien strains. This process of identification is termed as "kin recognition". By means of kin recognition, bacteria are able to employ different strategies to interact with the foreign cells. Such interaction may either be violent or symbiotic in nature. The nature of interaction depends on the ambient conditions of the growth medium as well as the interacting species. In general, when two different species of bacteria interact with each other, growth of the cells is inhibited due to cell death brought about by the competing species. An example of such interaction is observed between two adjacent colonies of *Myxococcus xanthus* and *Proteus mirabilis* where an interface forms between the two growing colonies which prevents the two colonies from coalescing [33]. When bacteria from the same species interact with each other, one may observe either inhibition or cooperation. Matsushita and co-workers found that when two colonies of *B. subtilis* interact with each other, if the growth medium is nutrient deficient, an interface forms [34], but they coalesce in rich nutrient environments [35]. Two colonies of *P. mirabilis* forms an interface between them if the colonies belong to different strains, but they coalesce if the strains are identical [29]. Identical strains of interacting *Paenibacillus dendritiformis* colonies may either form an interface or may coalesce depending on the morphotype [28]. Other examples of inhibitory interactions within identical or similar bacterial species include cannibalism (sporulating *B. subtilis*), suicide (*Staphylococcus aureus*) and fratricide (*Streptococcus pneumoniae*) [27, 55, 68].

2.4 Modelling Bacterial Colonies

The complex living nature of bacteria makes it challenging to accurately capture all the features pertaining to the growth and locomotion of the bacteria. Therefore, there exist numerous mathematical models each of which aims to capture certain aspects of bacterial growth. In liquid culture medium, the spatial distribution of bacterial cells is homogenous and the population count of the cells is more relevant to describe the kinetics of metabolic activities. In semi-solid growth media, however, the spatial distribution of cells constituting various colony morphologies is important. In this section, the different prominent models related to bacterial growth in liquid and on semi-solid media are described.

2.4.1 Bacterial Growth in Liquid Media

Bacteria divide by binary fission. In this reproductive process, a mother cell divides into two daughter cells. Therefore, in a nutrient-rich favourable environment where no adversities are present, the population of the bacteria would grow as a geometric sequence at each generation. Mathematically, if X_n is the population of the bacteria after the n^{th} generation, then:

$$X_{n+1} = 2X_n \tag{2.1}$$

After a large number of cell cycles, the growth rate of the bacteria can be defined as:

$$\frac{dX}{dt} = \frac{X_{n+1} - X_n}{\tau} \tag{2.2}$$

where τ is the generation time or the doubling time which is the duration in which the population doubles. For *E. coli*, under favourable conditions, $\tau \approx 20$ min. Combining (2.1) and (2.2), the final ordinary differential equation governing the demography of bacteria can be stated as:

$$\frac{dX}{dt} = \frac{X_{n+1} - X_n}{\tau} = rX \tag{2.3}$$

with a constant specific growth rate $r = 1/\tau$. This is the well-known Malthusian demographic model proposed by Thomas Robert Malthus in the eighteenth century [69-71]. According to Malthusian demographics, in a favourable environment, population of bacteria would grow exponentially, $X(t) = X_0 e^{rt}$, where X_0 is the bacterial population at $t = 0$. The Malthusian model assumes that the resources available to a species in the ecosystem are unlimited. This, along with absence of diseases, predators or any environmental deterrence, allows bacteria to grow unrestrained, resulting in exponential population explosion.

However, unrestrained population growth is physically unrealistic. Environmental factors and availability of resources have very important roles in determining the population dynamics of a system. In any environment, the amount of resources available to the growing population is limited and would deplete as the population continues to grow. Thus, in a limited environment, a population cannot grow freely. This is one of the outcomes of Darwin's theory of evolution. Darwinism dictates that in an environment with limited resources, the members will struggle for existence and only the fittest would be chosen by natural selection [72]. Limited resources would consequently lead to competition to survive. This indicates that the environment has a finite carrying capacity. As the population size increases, there is an increasing stress on the availability of resources and the ensuing struggle is instrumental in keeping the population growth in check. As a result, the specific growth rate r is a combination of the specific birth (a) and the mortality (b) rates, $r = a - b$. In a limited resource environment, the specific mortality rate will be governed by the population size; the larger the population, the greater the competition, and consequently, more

fatality. Considering the specific mortality to be a linear function of the population, $b(X) = b_0 X$, the specific growth rate $r(X)$ can be expressed as:

$$r(X) = a - b_0 X \tag{2.4}$$

The specific birth rate (a) of the system is considered to be a constant. While the specific death rate is affected by intra and interspecific competition, the specific birth rate is not, which justifies why it can be assumed to be a constant. Hence, the population dynamics is given by:

$$\frac{dX}{dt} = r_L X\left(1 - \frac{X}{K}\right) \tag{2.5}$$

This is the well-known logistic demographic equation proposed by Pierre Verhulst in the 19th century. r_L is the modified specific growth rate for the logistic model and K is the carrying capacity of the ecosystem which signifies the maximum population size that the ecosystem can sustain [73-75]. In terms of the specific birth and death rates, $r_L = a$ and $K = a/b_0$. Equation (2.5) shows that when resources are plentiful, or in other words, $X/K \ll 1$, the logistic equation reduces to the Malthusian demographics. However, after long periods of time, the growth rate $\frac{dX}{dt} \to 0$ and the population saturates.

The logistic (also known as Verhulst) model, although physically realistic, does not explicitly consider resource/nutrient depletion due to population growth. This may be important in cases where one would like to study the biodegradation of substrates by the bacteria. In 1949, Jacques Monod proposed an empirical function governing the nutrient limited specific growth rate $r_M(c)$ [76, 77]:

$$r_M(c) = r_0 \frac{c}{k+c} \tag{2.6}$$

where c is the nutrient concentration, k is the half saturation constant and r_0 is the maximum specific growth which signifies the specific growth rate when $c \to \infty$. In Monod's nutrient depletion model, the population growth, therefore, is given by:

$$\frac{dX}{dt} = r_M(c) X \tag{2.7}$$

The nutrient depletion is governed by the yield γ which denotes the amount of nutrient consumed per unit generation of bacterial biomass:

$$\frac{dc}{dt} = -\gamma \frac{dX}{dt} \tag{2.8}$$

It is easy to note that when nutrients are abundant, i.e., $c \to \infty$, the Monod's model reduces to the Malthusian model with specific growth rate r_0. In nutrient limited conditions, $r_M(c) \to 0$ and the population saturates. The saturation population according to Monod's model is $X(t \to \infty) = \frac{c_0}{\gamma} + X_0$ where c_0 and X_0 are the initial nutrient concentration and population size respectively.

Figure 2.5 compares the population growth predicted by the Malthusian, logistic and the Monod's models for the same specific growth rate, $r = r_L = r_0 =$ 3/h. The carrying capacity for the logistic curve $K = 0.964$. The Monod's parameter $\gamma = 16$ g/L is chosen such that both sigmoid curves have identical saturation populations. The half saturation constant $k = 10$ g/L. The sigmoidal Verhulst and Monod's models are able to replicate the growth curve of a bacterial culture over long times (Figure 2.3). Hence, these models are generally used for describing bacterial growth. Malthus'

model, although the simplest among the three, finds limited use because of its unrealistic assumptions. It, however, is useful in the log phase of the growth curve when the bacteria are most active. Therefore, the Malthusian model provides a simple way for estimating the log phase dynamics. Between the logistic and the Monod's models, the former has the advantage that it is a simple model which captures bacterial growth quite well. If one is only interested in the bacterial demographics rather than the nutrient consumption, the logistic equation is an ideal choice. But when the substrate depletion is a primary concern, Monod's model is usually used. In general, nutrient concentration governs several features associated with bacterial growth such as motility, sporulation, fruiting body formation. As a result, Monod's model finds wider applications when it comes to modelling bacterial growth. It is to be noted that none of the three models capture the death phase of the bacterial growth curve.

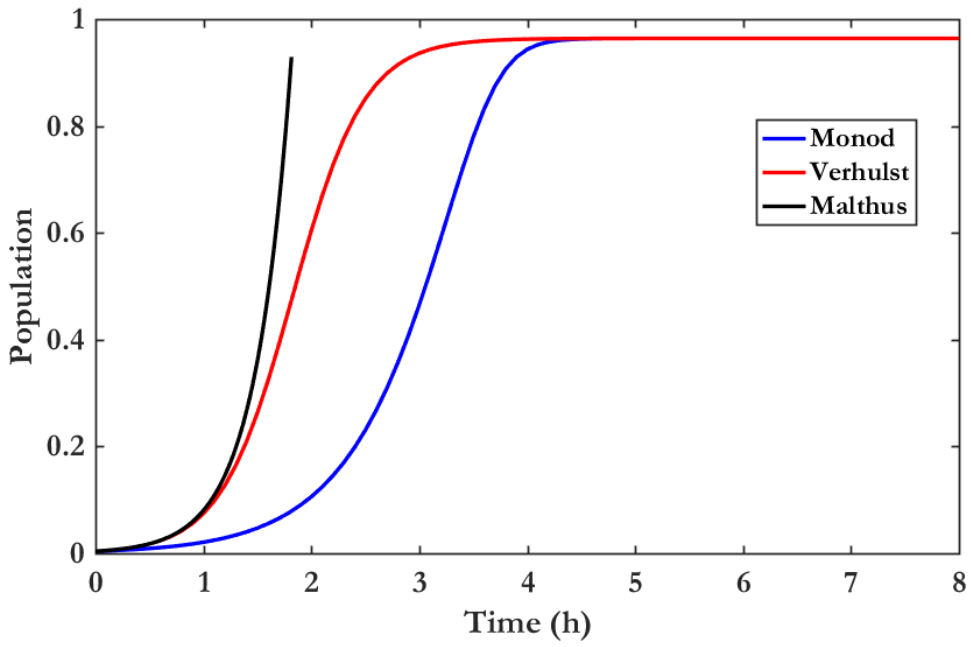

Fig. 2.5. Comparison between the Malthusian, Verhulst and the Monod models

2.4.2 Bacterial Colony Modelling

On a solid surface such as an agar plate, as bacteria grow by binary fission, they spread out in different directions in search of nutrients from the growth medium. The complex network of spreading bacteria forms the colony. Depending on the utility and focus of study, mathematical models of bacterial colonies can be classified into three broad categories:

- Hydrodynamic models
- Reaction-diffusion models
- Communicating walkers model

Hydrodynamic models

A bacterial colony can be regarded as a thin film of a complex active fluid spreading across the surface of a semi-solid growth medium. The multiphase fluid constituting the colony is viscoelastic in nature and contains bacterial cells dispersed in a liquid phase [37]. Hydrodynamic models typically consider three mechanisms: i) the growth of bacterial biomass in the complex thin film, ii) the osmotic influx of nutrient and water from the growth medium into the thin film, and (iii) the expansion of the thin film. Growth of bacterial population by binary fission increases the mass fraction of bacterial biomass in the complex film. As bacterial population increases, nutrient and water are consumed and this creates an imbalance of osmotic pressure between the colony and the growth medium. Consequently, more nutrient and water and drawn into the colony. Bacterial growth also increases the production of extracellular polymeric matrix inside the colony. The expansion of the thin film is driven by the combined effect of imbalance in osmotic pressure and bacterial growth. The expansion of the colony is often described by the Darcy's law and the Young-Laplace equation accounts for the wetting characteristic of the thin film [36, 37, 39, 42, 58, 78, 79]. Hydrodynamic models have been successful in reproducing the complicated morphologies exhibited

by bacterial colonies. Giverso et al. were able to generate the branching instabilities exhibited by colonies through their hydrodynamic model [58, 78, 79] as shown in Figure 2.6.

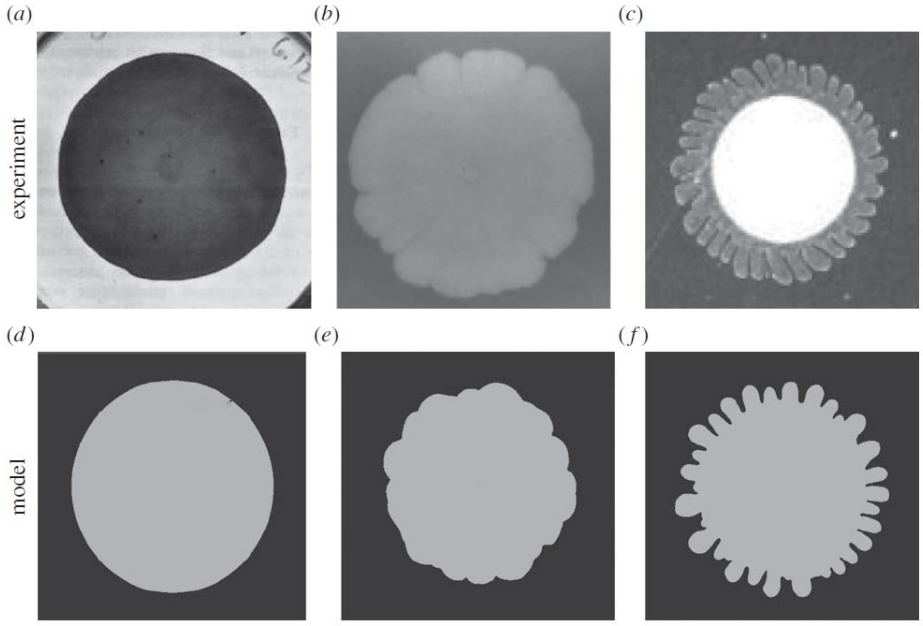

Fig. 2.6. Reproduction of experimentally observed bacterial colony morphologies (**a**, **b** and **c**) with numerically generated morphologies using hydrodynamic models (**d**, **e** and **f**) by Giverso et al [78]. Republished with permission of Copyright Clearance Center, from "Branching instability in expanding bacterial colonies", C. Giverso, M. Verani, P. Ciarletta, vol 12, issue 104, Copyright © 2015; permission conveyed through Copyright Clearance Center, Inc.

Hydrodynamic models are particularly useful when it comes to studying the influence of physical factors such as osmotic pressure, surface tension, viscosity and permeability of the growth medium. Seminara et al. incorporated the effect of osmotic pressure imbalance caused by nutrient uptake in a hydrodynamic model and quantitatively proved that osmotic spreading is controlled by extracellular matrix production [36]. Trinschek et al. used an evolution equation for thin films to study the effects of surface tension on osmotic colony spreading [37, 39, 42].

Reaction Diffusion Models

Bacterial colonies can be treated at as a dense network of cells which are continuously proliferating while at the same time navigating the surface of the growth medium in search of nutrition. As the bacterial cells moves outward radially, the colony spreads. Proliferation and spreading are often modelled using reaction diffusion (RD) models. It is assumed that bacterial proliferation occurs at the same rate as that in aqueous solution at the same temperature and pH. This assumption finds merit considering the fact that the semi-solid agar surface on which the colony spreads is wet and contains a thin layer of water. Hence, the growth models described in the preceding section can be used to model bacterial proliferation. This, in general, constitutes the reaction term. In some variations of the RD models, additional terms such as mortality, are introduced as a part of the reaction term. The diffusion term in the model accounts for the locomotion of the cells. Flagellar locomotion executed by bacterial cells is random in nature and resembles a Brownian type motion [80]. Such motion is driven by external stimuli such as chemotaxis, thermotaxis and phototaxis. Because of this randomness in motion, it is suitable to model the locomotion using a diffusion term. A typical RD equation is as follows:

$$\frac{dX}{dt} = rX + \nabla \cdot \left[D_b \nabla X \right] \tag{2.9}$$

Here r is the specific growth rate of the bacteria and D_b is the diffusion coefficient governing colony spreading. The parameter r can be defined differently depending on the growth model. For Malthusian growth, r is a constant and for logistic growth model, $r = r_L \left(1 - \frac{X}{K} \right)$. For nutrient limited growth, $r = r_M \left(c \right)$ according to the Monod's model. In this case, an additional equation is necessary to account for transport of nutrients from the growth medium towards the colony where it is consumed, as shown below:

$$\frac{dc}{dt} = -\gamma r_M(c) X + \nabla \cdot [D_c \nabla c] \tag{2.10}$$

where D_c is the diffusion coefficient of the nutrients. The coupled set of equations (2.9) and (2.10) are useful in estimating the biodegradation of the nutrient. In the case of enzyme mediated degradation of substrates which are not metabolized by the bacteria for energy, Michaelis-Menten kinetics is invoked instead of Monod's nutrient depletion model as in (2.10) [81].

The spreading characteristics of the colonies are quite complicated to model mathematically as bacterial motility is very sensitive to environmental conditions such as temperature and pH, rheology of the growth medium, type and availability of the nutrient source, as well as presence of predators and alien colonies. These factors not only influence the morphology of the colony, but also the rate of spreading. To incorporate the effect of these factors, the diffusion coefficient of the colony D_b is treated as a function of these factors. In fact, a constant D_b alone cannot numerically produce the branching instabilities associated with some colony morphologies. By using variable D_b , and/or accompanied by a mortality term, one can successfully reproduce complex colony morphologies using RD models [82] as evident from Figure 2.7.

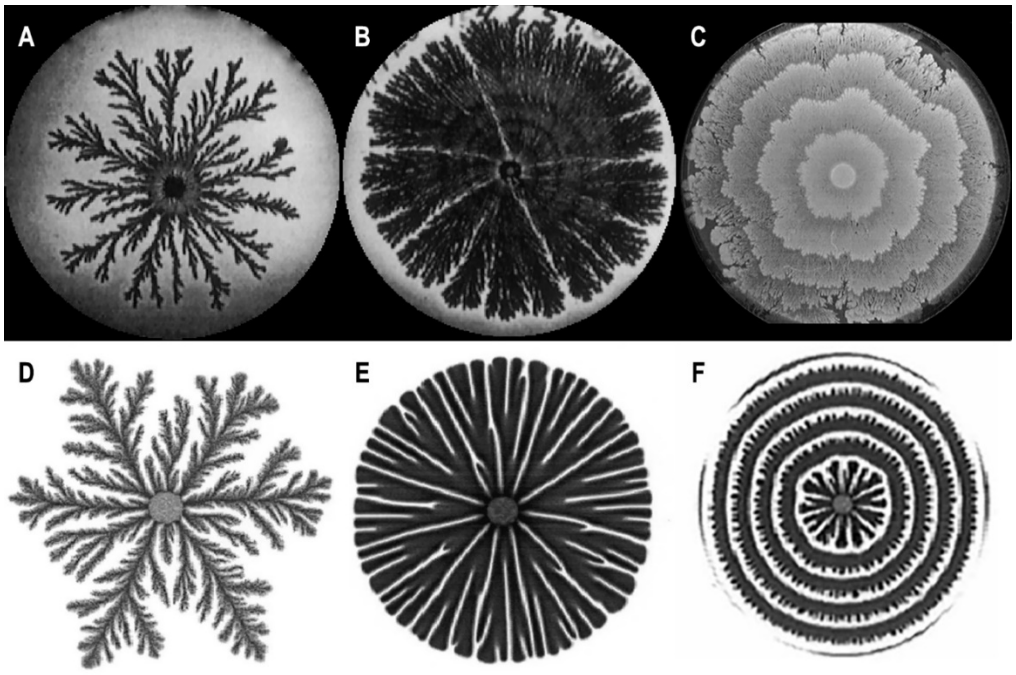

Fig. 2.7. Reproduction of experimentally observed bacterial colony morphologies (**A**, **B** and **C**) with numerically generated morphologies using RD models (**D**, **E** and **F**). Reprinted from Physica A-Statistical Mechanics and Its Applications, Vol 260, no. 3-4, I. Golding, Y. Kozlovsky, I. Cohen, E. Ben-Jacob, "Studies of bacterial branching growth using reaction-diffusion models for colonial development", pp. 510-554, Copyright © 1998, with permission from Elsevier.

The advantage of RD models over hydrodynamic models is that RD models are quite simple and easy to solve numerically. However, unlike hydrodynamic models it is not trivial to incorporate the effects of other factors such as osmotic pressure and surface tension. Also, these models often use empirical relations for the mortality and diffusion coefficients to explain specific characteristics of the colony [82]. Therefore, these models are not suitable for depicting colonies from a physical viewpoint. But because of their simplicity, RD models are a popular choice when it comes to modelling bacterial colonies.

Communicating walkers model

The communicating walkers (CW) model was developed by Ben-Jacob and co-workers in the 1990s [80, 83, 84]. Like the RD models, the CW model is based on the premise that bacteria execute random motion driven by chemotaxis to derive nutrition. As the bacteria spread, they proliferate thereby growing in population. Unlike the RD models, the CW model considers the cooperation between cells to survive in adverse growth conditions. The CW model is a discrete model which considers coarse graining of cooperating bacterial clusters (termed as "walkers"). These walkers communicate with each other as they move. The CW model is particularly useful in studying the behaviour of bacteria in nutrient deficient environments when locomotion is heavily restricted. In such situations, the CW model produces diffusion limited aggregates which agree with experimental observations very well. In nutrient rich environments, CW model generates compact morphologies as is observed experimentally [80]. Figure 2.8 demonstrates the utility of the CW model. Figures 2.8a and 2.8b show branching morphologies in *B. subtilis* colonies on 2% agar plates containing 0.5 g/L and 0.25 g/L of peptone (nutrient source) respectively. Denser branches occur at lower peptone concentration due to enhanced chemotactic signalling. Figures 2.8c and 2.8d are able to replicate these morphologies very accurately. Figure 2.8c is generated without incorporating chemotactic signalling into the CW model. But on turning on chemotactic signals between walkers, the branches become denser (Figure 2.8d), thereby agreeing with the experimental observation.

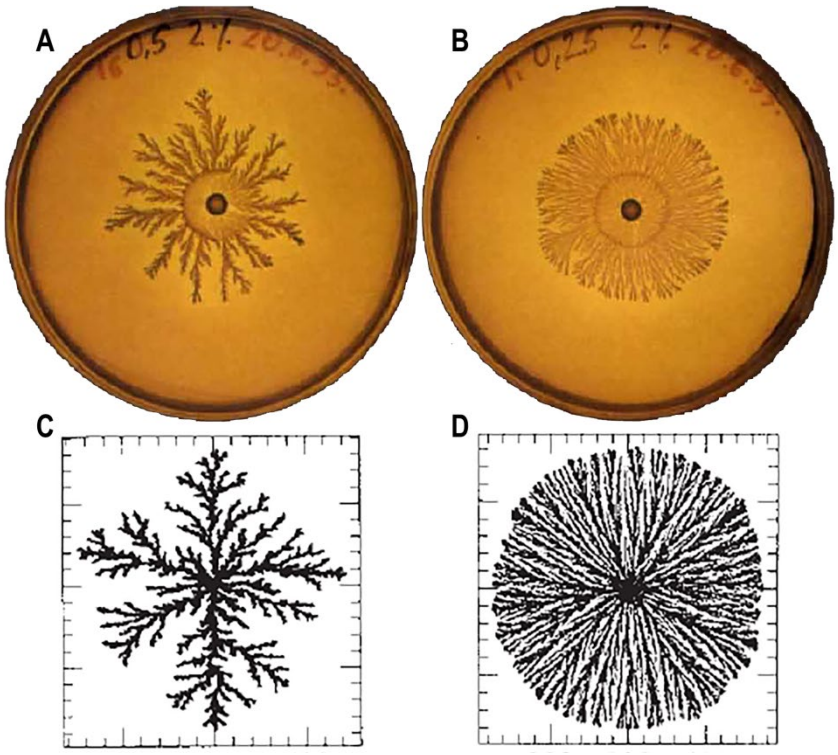

Fig. 2.8. Reproduction of experimentally observed bacterial colony morphologies (A, B and C) with numerically generated morphologies using CW models (D, E and F). Reprinted by permission from Springer Customer Service Centre GmbH: Nature [80], Copyright © 1994.

2.5 Knowledge Gap

Interaction patterns between different bacterial colonies are ubiquitous in nature. However, very limited scientific literature exists on the study of inter-colony interactions in bacteria. The most prominent work on this topic was performed by Be'er and co-workers. They studied the interface formation between *Paenibacillus dendritiformis* colonies in a low nutrient environment. Their study showed that the interface formation between colonies is brought about by production of certain biochemical inhibitors by each sibling colony in response to the other [4]. These inhibitors diffuse through the growth medium and cause cell death at the approaching colony fronts. They were able

to isolate the inhibitor molecules and found that inhibition occurred only when the concentration of these inhibitor exceeds a certain lethal concentration. This is shown in Figure 2.9.

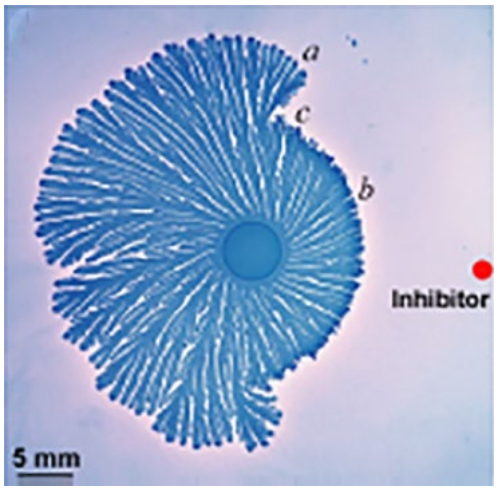

Fig. 2.9. Biochemical inhibition in *P. dendritiformis* colony due to presence of inhibitors [4]. The region *a* has normal growth where the concentration of the inhibitor is lower than the lethal concentration. The region *b* shows inhibited growth where high concentration of inhibitors is present. Region *c* is the transition zone.

By varying the nutrient, agar concentrations and the separation between the colonies they found that these parameters affect the progression of the colony fronts as the two colonies interacts. However, the exact roles of these parameters were not investigated. They also found that even at very small separations between the colonies, an interface always formed and coalescence was not reported. Later, Be'er at al. identified the protein molecules which cause inhibition [44]. The molecular weights of these biomolecules were found out to be of the order of 10^4 g/mol. Based on the diffusion of these inhibition factors, they proposed a mathematical model to simulate the interface formation. Chakraborty et al. echoed the findings of Be'er et al. They found that two different bacterial species (*Bacillus cereus* and *Pseudomonas sp.*) exchange biochemical signals to form a zone of inhibition between the two colonies [32]. They also proposed a mathematical model to

numerically simulate the inhibitory interaction. The models proposed by Be'er et al. and Chakraborty et al. incorporated the diffusion of inhibition factors through the growth medium which cause biochemical inhibition. Due to lack of sufficient understanding of inter-colony interactions, mathematical models of the phenomenon are scarce and specific to the problem being studied. Other than the above models, Wakita et al. reproduced the coalescence in *B. subtilis* colonies using their RD model [35]. Their model did not include an interaction term but instead consider independent growth and coalescence of the two colonies. Patra et al. introduced a mortality term in their RD model to study the interface formation between colonies of two different bacterial species specifically, *Myxococcus xanthus* and *Proteus mirabilis* [33]. Unlike Be'er et al., they did not explicitly account for diffusion of inhibition factors in their model. Although Wakita et al. reported coalescence in *B. subtilis* colonies in nutrient rich environments, they did not investigate the interactions experimentally in detail.

Till date, most of the studies pertaining to interactions between colonies have been limited to investigation of biochemical factors which influence interface formation. As stated earlier, physical factors also play important roles in determining the spreading characteristics of colonies. For better understanding of the biophysics of interacting bacterial soft matter, it is essential to study the influence of physical processes on the nature of interaction between colonies. However, this area remains largely unexplored and forms the motivation for this thesis. Recognizing that the concentration of agar in the growth medium indirectly modulates the governing physical processes, it has been chosen as one of the experimental parameters for the study. To understand the influence of colony maturity, the center-to-center separation between the colonies has been adopted as the second parameter. The bacterial species of choice is *Bacillus subtilis* because of its swimming and swarming motility over semi-solid agar media and its wide applications in bacteriological studies. The experimental component of the thesis involves a detailed parametric study of the inter-colony

interaction dynamics in *B. subtilis*. This is supplemented by experiments aimed at understanding how agar influences colony spreading in single *B. subtilis* colonies. Finally, a third set of experiments have been performed to determine how a *B. subtilis* colony interacts with a physical impediment. In this study, oil drops and solid walls/discs have been used as physical simulacra of the second colony. The mathematical modelling component of the thesis complements the experimental results. Although there are models capable of reproducing interfaces and coalescence between colonies, none of the existing models capture both interactions in the same model, i.e. the models either simulate an interface or coalescence. The existing models fail to reproduce the experimental observations where both interaction patterns have been found to occur under different combination of the experimental parameters. In thesis, a model has been proposed which numerically simulates both patterns and enables one to predict the nature of interactions based on the values of the parameters.

Chapter 3
Experimental Materials and Methods

Chapter 3 describes in detail the conditions, materials and species of bacteria used in the experiments. The different experiments performed in the present study are tabulated in an experimental matrix. Techniques used for analysis of experimental data are also mentioned.

3.1 Materials and Micro-organisms

Miller's Luria Broth (LB) base (Bector, Dickinson and Company, 241420, containing 10 g/L pancreatic digest of casein, 5 g/L yeast extract and 0.5 g/L sodium chloride) was purchased from Fisher Scientific, Canada. Bacteriological agar was purchased from Sigma-Aldrich (A5306-250G, Canada). Bacterial strains *Bacillus subtilis* (ATCC© 6633) and *Escherichia coli* (ATCC© 25922) were purchased from American Type Culture Collection (ATCC©), Manassas, USA. Another bacterial species *Pseudomonas fluorescens* (CHA0) was generously given by Dr. Howard Ceri, Biofilm Research Group, Department of Biological Sciences, University of Calgary.

Polydimethylsiloxane (PDMS, Sylgard 184, Dow Corning, NY, USA) and Polypropylene (PP, cut out from Thermo Fisher Scientific Centrifuge Tubes) were used to fabricate cuboid and circular discs as substitutes for one of the colonies. The dimensions of the PDMS cuboid structures were 24 mm x 6 mm x 3 mm, and for PP, they were 30 mm x 5 mm x 1 mm. The diameter of the PDMS discs was 10 mm and height was 3 mm. For the PP discs, the diameter and height were 10 mm and 5 mm respectively. Commercial castor oil was used as a liquid substitute for a bacterial colony. Castor oil is highly viscous and has a molecular weight of 927 g/mol. Therefore, there is negligible diffusion of a sessile castor oil droplet on agar medium and can be used as a liquid

substitute for a bacterial colony. 1 μL of castor oil droplets were drop casted on the surface of agar on petri-dishes.

3.2 Preparation of Growth Medium

Miller's Luria Broth (LB) base was mixed with bacteriological agar to prepared solid nutrient rich medium for B. subtilis colony growth. Throughout the study, the concentration of LB in the growth medium was held constant (1.5%) while the concentration of agar was varied from 0.5% to 5% (w/v). The LB-agar solution was then autoclaved to prepare a sterile homogenous growth medium. The mixture was then poured to petri-dish (diameter 90 mm) and cooled down to room temperature before bacterial inoculation.

3.3 Bacterial Culture Preparation

For each experiment, a fresh pre-culture of the *B. subtilis* was prepared in 1.5% LB broth and incubated for 16 hours. The incubation temperature was maintained at 37°C for *B. subtilis* and *E. coli* cultures, while 30°C for *P. fluorescens*. Each bacterial colony was then prepared on an LB-agar plate by drop casting of 1 μL of bacterial culture, and incubated at corresponding incubation temperatures. To maintain the bacterial cell density, the inoculum size was controlled by cell count. Every 16-hour pre-culture contains 1.4×10^6 viable cells/ml with an optical density (at 600 nm) of 0.6 $\pm$ 0.02. The experimental deviation on cell count is calculated to be 0.4×10^6 /ml which represents ~28% uncertainty in repeatability of bacterial cell count. It can be assumed that the experimental inoculum (1 μL) contain around 1×10^3 viable cells.

3.4 Experimental Design

Three different sets of experiments were performed to study radial growth pattern with *B. subtilis* during - i) two sibling colony interaction; ii) no interaction (single colony radial growth pattern) and iii) interaction with physical material such as PDMS and castor oil. The first involved inoculating

two sibling *B. subtilis* colonies on an agar plate. The concentration of agar in the growth medium was varied from 0.5% to 5% (w/v). During inoculation of the colonies by drop casting, the distance between the centers of the drops was varied in steps of 10 mm from 10 mm to 30 mm. This initial separation between the colonies and the concentration of agar in the growth medium were chosen as two parameters for the experiments. In the second set of experiments, a single colony was used to study the radial growth rate of *B. subtilis* colonies as a way to determine the diffusion coefficient of *B. subtilis* on agar when physical and biological interaction is absent. The concentration of agar was also varied between 0.5 and 5% (w/v). To collect data at equal intervals of time, two parallel sets of experiments were conducted, which were inoculated 12 hours apart. The third set of experiments was performed to study the interaction of *B. subtilis* colonies with physical objects. A sessile castor oil droplet as a liquid substitute, and PDMS and PP walls and discs as solid substitutes were used for replacing one of the sibling colonies. A *B. subtilis* colony was inoculated at a distance of 10 mm from the nearest edge of the sessile oil drop or PDMS/PP wall or disc. In these experiments, agar concentration was fixed at 1.5% (w/v). In all three sets of experiments, the nutrient concentration in the growth media was held constant at 1.5% (w/v) (or 15 g/L).

Experimental observations were found to be sensitive to the changes in experimental conditions but under identical protocols they were reasonably repeatable. The uncertainty of bacterial cell count resulted into the effective colony diameter deviation between 5% and 36% recorded on 1% agar over a period of 36 hours post inoculation. For higher concentration of agar media, the deviation was considerably smaller. For 1.5% agar, the deviation was between 15 - 23% and for 2, 3 and 5% agar media these were between 3-22%, 1-5%, and 2-22%, respectively.

Table 2.1 summarizes the experimental matrix for the present study.

Table 2.1. Experimental Matrix

Experiment	Objective	Bacterial Species	Parameter Range
Single Colony	Study role of agar, Estimate parameters	*B. subtilis*	Agar: 0.5 – 5.0%
Single Colony with Obstacles	Influence of physical barriers on interactions	*B. subtilis*	Agar: 1.5% Separation: 10 mm
Two Colonies	Nature of inter-colony interactions	*B. subtilis,* *E. coli,* *P. fluorescens*	Agar: 0.5 – 5% Separation: 10 – 30 mm

3.5 Data Collection and Analysis

The growing bacterial colonies were recorded using a Nikon D3400 digital single-lens reflex (DSLR) camera with an 18-55 mm lens mounted on a tripod stand. The background illumination was provided using intensity adjustable 4" x 4" white LED backlight (Edmund Optics, Stock# 88-504). The petri-dishes were monitored at regular intervals of time to generate a uniform set of data. Microscopic images of the growing colonies were taken using a Nikon Eclipse Ti inverted microscope. The images were processed in MATLAB® (MathWorks®), using the inbuilt image processing toolbox, to obtain the size of the colonies.

The diffusion coefficient of the nutrient, a parameter required in the theoretical model, was estimated using Coomassie blue dye which has a molecular weight of 826 g/mol. 1 μL of the dye was allowed to spread on the surface of the growth medium on a petri-dish. Since the thickness of the agar in the petri-dish is insignificant compared to the diameter of the petri-dish (~4%), the dye

diffusion is assumed to occur only on the agar surface. The intensity of color of the spreading dye was used as the indicator of dye concentration in the image processing. For estimating the growth parameters of *B. subtilis*, Origin® (OriginLab®) was used to fit the experimental growth curve for a single colony with the theoretical model. This will be discussed in the next chapter.

Chapter 4
Growth of Single Bacterial Colonies

In this chapter, results from single *B. subtilis* experiments are described. A mathematical framework for single colonies is formulated, and the role of agar of growth of colonies is elucidated from a quantitative level. Relevant model parameters pertaining to single colony experiments are estimated.

4.1 Role of Agar in Colony Spreading

Colony spreading is controlled by physical factors such as osmotic pressure [36-38], surface tension [15, 39, 40, 42, 56], viscous drag and permeability of growth medium [43]. All of these physical factors are affected by the agar concentration in the growth medium. Agar is a mixture of biopolymers derived from the cell walls of red algae. It is widely used in microbiological studies for preparing bacterial cultures. Solution of bacteriological agar and a source of nutrients, when autoclaved at around 120ºC produces a hydrogel on which bacterial colonies can grow. Agar gel consists of a network of pores which allows the transport of water and nutrients and is ideal for growing bacterial colonies. The concentration of agar in the hydrogel determines the pore size and therefore, significantly alters the rheological properties of the gels. At low concentrations, the agar gel is highly porous with large pores. As the concentration increases, the pore size drastically reduces [51], and the hardness of the agar gel increases. This change affects bacterial motility and thereby influences the rate of colony spreading on agar plates. The soft and wet surface of agar at low concentrations is favourable for bacterial locomotion, whereas the hard and dry agar surface at high concentrations presents an unfavourable environment for bacterial locomotion. To quantify the rheological change in agar gels, the Young's moduli of agar gel samples were measured in an

ElectroForce® 3200 Series III compression testing machine for different agar concentrations between 1% and 5%. The samples of agar gel were prepared by autoclaving a solution of 1.5% LB and the requisite amount of agar and made into 15 mm cubes. The cubic samples were subjected to small compressions (linear strain $\Delta l/l < 0.067$) under loads ranging from 50 mN for 1% agar samples up to 2.5 N for 5% samples. To ensure the statistical reliability of the compression tests, each sample was tested thrice. As the deformations of the samples were small, the compressive stress on the samples could be approximated as $\sigma \approx F/A$ where F is the compressive load on the sample and A is the cross-sectional area of the undeformed sample. Similarly, the strain can be approximated as $\varepsilon \approx \Delta l/l$ where Δl is the displacement and l is the height of the uncompressed sample. Therefore, the Young's modulus can be defined as the slope of the $\sigma - \varepsilon$ curve: $E \approx \sigma/\varepsilon = Fl/(A\Delta l)$. To estimate the Young's modulus of the samples, the experimental load-displacement curves are fitted with a straight line in Origin® and the slope of this line m is calculated, and $E = ml/A$. It is to be noted that as the samples are not perfectly elastic, the $F - \Delta l$ curves are non-linear at the beginning of the compression. Hence, the slope of the curve is computed between points where the curve is roughly linear. Figure 4.1 shows an experimental $F - \Delta l$ curve for one of the 5% agar samples. The red line is the best fit straight line whose slope is related to the Young's modulus of the sample.

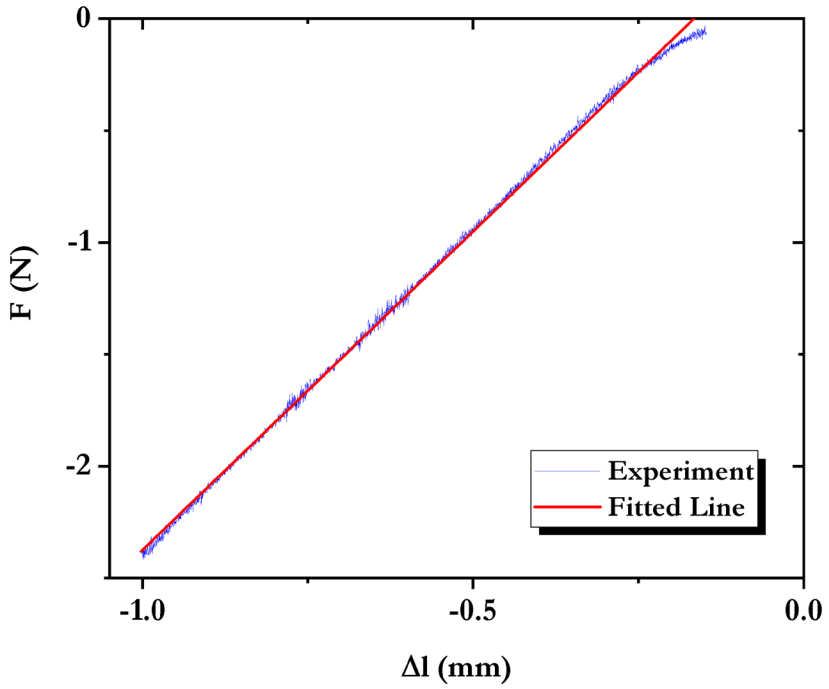

Fig. 4.1. Load vs displacement curve obtained experimentally for 5% agar sample is fitted with a straight line to estimate the Young's modulus for the sample.

The Young's modulus estimated was found to increase monotonically with agar concentration as shown in Figure 4.2. The standard deviation in estimation of the Young's modulus lies between 3% and 12% and is within acceptable range of accuracy.

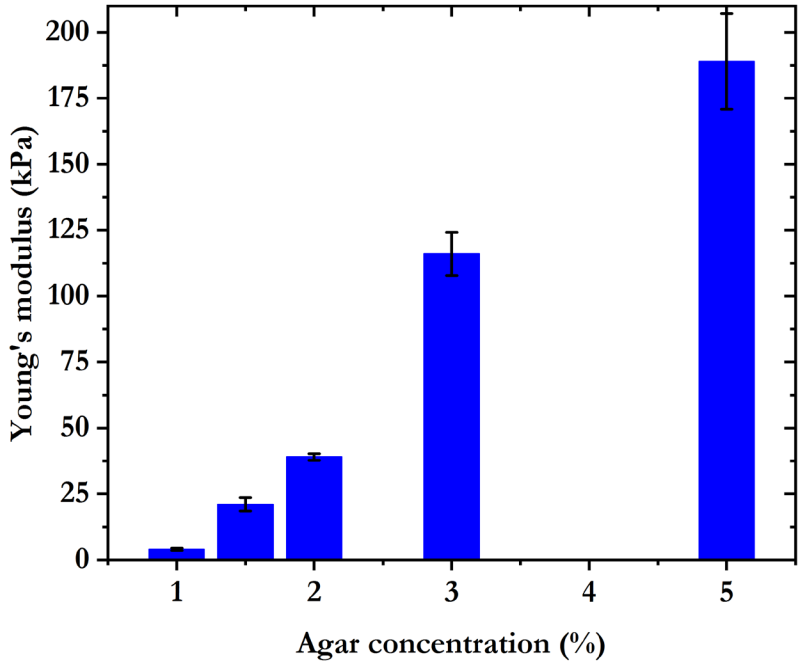

Fig. 4.2. Variation of the Young's modulus of agar gels at different concentrations.

Agar concentration influences the colony growth and morphologies as discussed in chapter 2. To elucidate the role of agar on colony spreading, single colonies of *B. subtilis* were grown on agar plates with 1.5% nutrient. The agar concentration was varied from 0.5% to 5%. The standard concentration in bacteriological experiments is 1.5% or less. By changing the agar concentration, the rate of spreading of the colonies was found to vary quite significantly. Figure 4.3 shows the growth and spreading of single colonies over time at 0.5%, 2% and 5%.

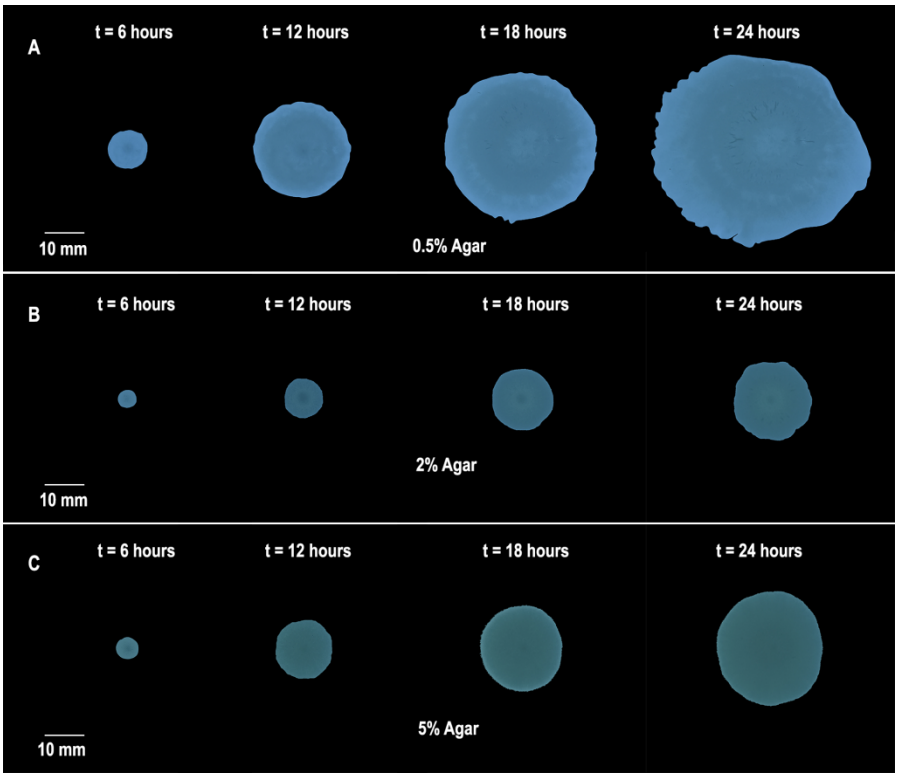

Fig. 4.3. Spreading of B. subtilis colonies on agar plates over time on **(A)** 0.5% agar, **(B)** 2% agar and **(C)** 5% agar.

To compare the radial spreading of the colonies, an effective diameter of the colony d_{eff} has been defined based on the area A covered by the colony as $d_{eff} = \sqrt{4A/\pi}$. In Figure 4.4, the effective colony diameter has been plotted at different agar concentrations at various time points post inoculation.

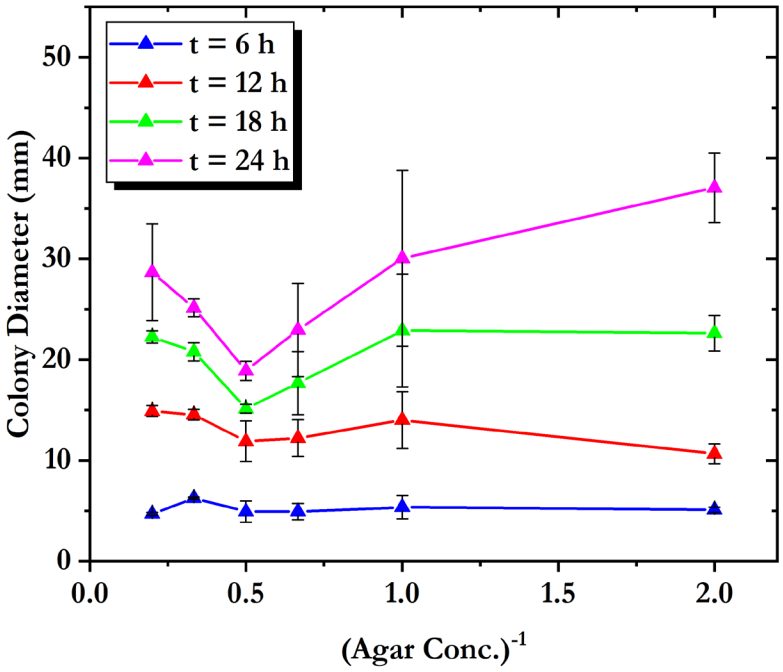

Fig. 4.4. Effect of agar concentration of the rate of radial spreading of *B. subtilis* colonies on the surface of agar plates.

Figure 4.4 shows that at 6 hours, the colonies have similar diameters. But over time, the colonies growing on 0.5% agar spread much faster than those growing on higher agar concentrations. The rate of spreading decreases on increasing agar concentration from 0.5% till 2%. Beyond 2%, again there is an increase again in the rate of spreading at 3% and 5% agar concentration. Increase in the colony spreading rate at very high agar concentrations (3% and 5% agar) may be because of increased production of surfactin which is a biosurfactant unique to *B. subtilis*.

The experiments with single colonies confirm that agar plays an important role in the spreading of the colonies and shows that low agar concentration environments favour bacterial motility and colonies spread faster as compared to high agar concentration environments. In terms of mathematics, the effect of agar can be incorporated into the diffusion coefficient of the colonies.

To study the effect of agar on a quantitative level, a reaction-diffusion model has been used to numerically simulate the colony spreading which is described in the following section.

4.2 Mathematical Model

The spreading of single *Bacillus subtilis* colonies on agar plates is modelled using nutrient dependent reaction-diffusion equations as described in chapter 2. The growth of population of bacteria inside the colony is described by Monod's nutrient depletion model. The spreading of the colony on the surface of the growth medium is described by a two-dimensional diffusion term with a diffusion coefficient D_b defined for the colony. The nutrient transport is governed by the consumption inside the colony which creates a spatial concentration gradient that drives the nutrient towards the colony. As the colony grows, the consumption of nutrients creates a depletion zone around the bacterial colony. The depletion of nutrients attenuates bacterial metabolism which hampers energy production in the cells and thereby reduces the motility of the bacteria inside the colony [80]. In terms of mathematics, the diffusion coefficient of the colony is a function of the nutrient concentration $c(t,R,\theta)$ (R,θ are polar coordinates). Patra et al. suggested a simple augmentation to the diffusion term in the generalized RD equation (2.9) by the use of a step function for describing the nutrient concentration dependence of the diffusion coefficient. The modified diffusion coefficient $D_b^*(c)$ is expressed as [33]:

$$D_b^*(c) = D_b \mathcal{H}[c - c^*] \tag{4.1}$$

Here $\mathcal{H}[x]$ is the Heaviside step function. Physically, equation (4.1) signifies that where the nutrient concentration falls below a critical concentration c^*, bacterial motility will be arrested. D_b on the right side of equation (4.1) is a constant for a given agar plate, and will henceforth be addressed as

the diffusion coefficient of the colony. The coupled set of equations describing the colony spreading and nutrient transport is, thus, given by:

$$\begin{aligned}\frac{\partial X}{\partial t} &= r(c)X + \nabla\cdot\left(D_b\mathcal{H}\left[c-c^*\right]\nabla X\right)\\ \frac{\partial c}{\partial t} &= -\gamma r(c)X + \nabla\cdot\left(D_c\nabla c\right)\end{aligned} \tag{4.2}$$

Here, $X(t,R,\theta)$ is the bacterial population density. $r(c) = r_0\dfrac{c}{k+c}$ is the nutrient dependent specific growth rate according to Monod's model, with r_0, k and γ being the growth parameters as described in chapter 2. D_c is the diffusion coefficient for the nutrient transport. For the single colony model, it is assumed that the Monod growth parameters are identical to that of bacteria growing in a liquid culture medium. Hence, these model parameters will be estimated from growth curves generated in liquid culture of *B. subtilis* in 1.5% LB growth medium. To take advantage of the radial symmetry of the problem, a polar coordinate system is chosen with the origin defined at the center of the bacterial colony, and the angular dependences of c and X are omitted. The bacterial colony is inoculated in the form of a drop casting on the surface of the agar plate, and initially, the nutrient is homogenously distributed in the growth medium. The initial conditions, therefore, can be formulated as:

$$\begin{aligned}X(t=0, R\le\rho) &= X_0\\ c(t=0,R) &= c_0.\end{aligned} \tag{4.3}$$

Here, ρ is the radius of the drop cast. The domain of simulation is a circle of radius ρ_p (to simulate a circular petri-dish) $(\rho_p \gg \rho)$ with the origin of the polar coordinate frame fixed at the center of the domain as shown in Figure 4.5. At the boundary (Γ) of the simulation domain, no-flux

boundary condition is enforced for the bacterial population density and the concentration of nutrients is a constant:

$$\nabla X \cdot \hat{\mathbf{n}}\big|_{\Gamma} = 0$$
$$c\big|_{\Gamma} = c_0 \tag{4.4}$$

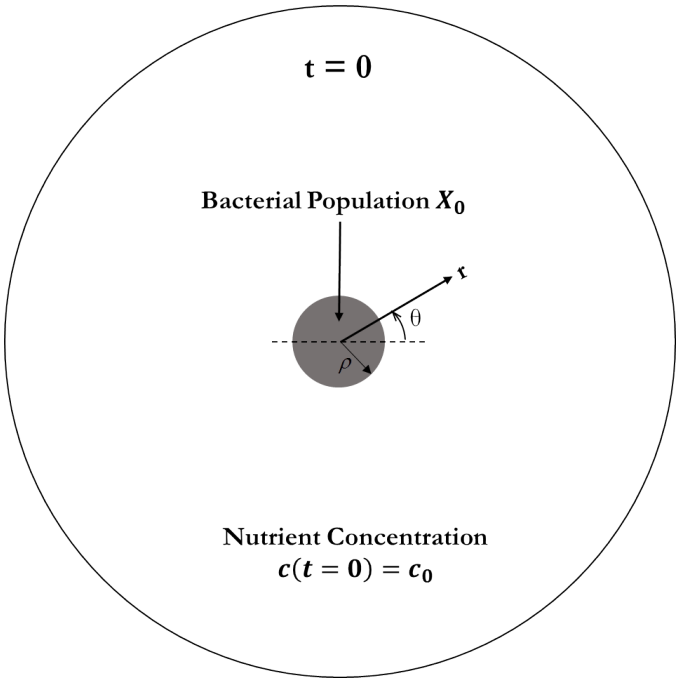

Fig. 4.5. Schematic showing the domain of numerical simulation at t = 0. The bacterial colony is inoculated in the form of sessile drops of radius ρ (in grey) with initial bacterial population X_0. The initial nutrient concentration in the growth medium is uniform.

4.3 Numerical Results

In order to quantitatively describe the role of agar on the rate of colony spreading, it is necessary to determine the dependence of the colony diffusion coefficient on the agar concentration. This is done by comparing the results obtained from the single colony experiments with the single colony

model (eqns. (4.2)) to estimate the parameter D_b. In order to solve eqns. (4.2), the growth parameters and nutrient diffusion coefficients are first required to be estimated. In this section all relevant model parameters are estimated. The growth parameters and the diffusion coefficients of the colony and nutrients will be necessary in solving the two-colony model which will be formulated in the next chapter.

4.3.1 Growth Parameters

The three parameters related to growth of bacterial population (r_0, k, γ) are estimated by comparing the experimental growth curve of a bacterial population with the theoretical model proposed by Monod. To do that a culture of *B. subtilis* is prepared in 1.5% LB solution and the population density of bacteria in the solution is recorded in terms of its optical density (OD) at 600 nm wavelength. The growth curve obtained from the experiments is shown in Figure 4.6. The experiment is repeated 3 times and the standard deviation in the measurement of the population density is less than 10% at all times $t \geq 3$ h post inoculation. Large errors exist earlier than 3 hours which can be attributed to the small values of the population density recorded at those time points. The yield γ is obtained from the relation described in chapter 2 from the saturation population density: $\gamma = \dfrac{c(t=0)}{X(t\to\infty) - X(t=0)}$. The initial nutrient concentration $c(t=0)$ = 15 g/L. The initial and saturation bacterial populations are obtained from the experimental growth curve. The remaining two parameters r_0 and k are consequently estimated by fitting the growth curve with the numerical solution of the Monod's model. In this regard, an approximate estimate of r_0 can be obtained from the log phase of the experimental curve. The $\log\left(\dfrac{X(t)}{X(t=0)}\right)$ vs t curve is approximately linear in the log phase of the growth curve, and the slope of the linear region gives an estimate of r_0. The

final estimate of r_0 and k are obtained from the numerical solution which best fits the experimental curve. In this case, the quality of the fit calculated in terms of the coefficient of determination $R^2 \approx 90\%$. Figure 4.6 shows experimental *B. subtilis* growth curve fitted with the numerical solution.

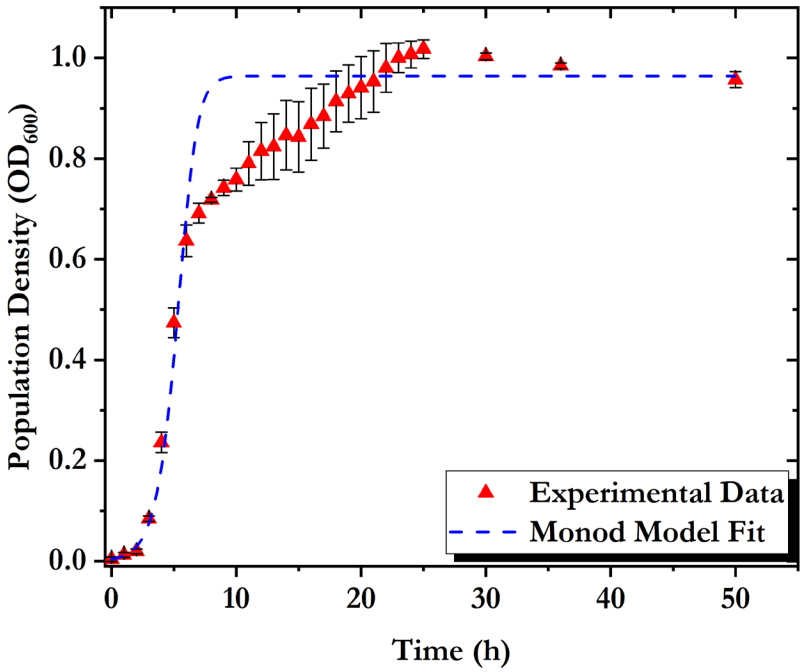

Fig. 4.6. Experimental growth curve of *B. subtilis* in 1.5% LB solution is fitted with the Monod's model to estimate the growth parameters.

It is assumed that the bacterial population growth on agar surfaces will be identical to that in culture solution. This enables the use of the estimated growth parameters in the formulated single colony model. The reason for this accommodation is that it is very difficult to estimate the growth parameters directly from growing colonies with reasonable degree of accuracy.

4.3.2 Nutrient Diffusion Coefficient

The nutrient source (LB) that is used in the experiments consists of a range of different molecules, starting from simple molecules as NaCl to large polymeric protein chains. The molecular weights of the component chemicals vary from 58.5 g/mol to around 2000 g/mol. Based on their molecular weights, each molecule diffuses at different rates. Smaller molecules diffuse faster than large polymers. In a nutrient rich medium such as in the present study, the dynamics of the nutrients will be governed by the slower large molecules. Hence, the effective diffusion coefficient of the nutrient will correspond to that of the massive protein molecules which diffuse very slowly through the growth medium. To estimate the order of magnitude of the effective diffusion coefficient of the nutrient source, Coomassie blue dye (molecular weight 826 g/mol) has been used and rate of spreading of the dye over the surface of the growth medium is measured. This was carried out in different growth media by varying the agar concentration from 0.5% to 5%. Figure 4.7 shows the spreading of the dye over time on 3% agar medium.

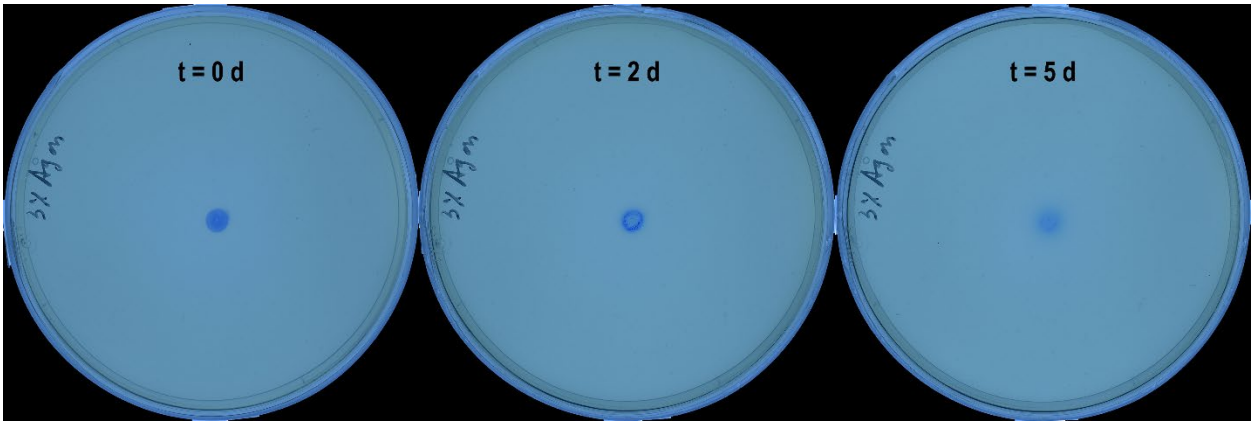

Fig. 4.7. Diffusion of Coomassie blue dye on 3% agar, 1.5% LB growth medium.

Figure 4.7 shows that at t = 0, the sessile dye drop is homogenous, but at t = 2 d, a ring forms with a high concentration of the dye present at the edge of the ring and the concentration of

the dye decreases towards to the center ("coffee ring" effect) [85]. Over time, the dye particles diffuse into the agar and the ring disappears beyond t = 5 d. The formation of the ring can be explained by considering the disparity in the transport of water and dye molecules through the agar medium. Water (mol. wt. 18 g/mol) is considerably lighter than the dye molecules, and as a result, the water molecules in the sessile drop (at t = 0) diffuses much faster than the dye molecules. In fact, the water in the sessile drop diffuses completely through the agar medium in less than 3 hours. The diffusion of the water molecules takes place from the edge of the sessile drop and leaves behind the dye molecules at the edge of the drop, thereby forming the ring that is seen at t = 3 d. Finally, the heavy dye molecules diffuse over a period of days.

The dye intensity has been correlated to the dye concentration in MATLAB® to determine the spatial distribution of the dye on the agar plate. It is assumed that the concentration of dye is uniform at t = 0, which means that the dye intensity at t = 0 in the sessile drop is constant, say I_0. Subsequently, the dye concentration at later times is generated by obtaining a spatial distribution of the dye intensity $I(R)$, and expressing it in terms of a normalized intensity distribution, $I(R)/I_0$. Figure 4.8 shows the distribution of the normalized intensity corresponding to the images in Figure 4.7. The dye concentration appears to be nearly constant inside the sessile drop at t = 0. The sharp peak corresponding to t = 2 d is indicative of the ring formation with dye molecules accumulating at a narrow radial location. In fact, the radial location of the peak can be taken as the radius of the dye ring which is very similar to the initial radius of the sessile drop. Finally, at t = 5 d, there is diffusion of dye into medium as was observed in Figure 4.7.

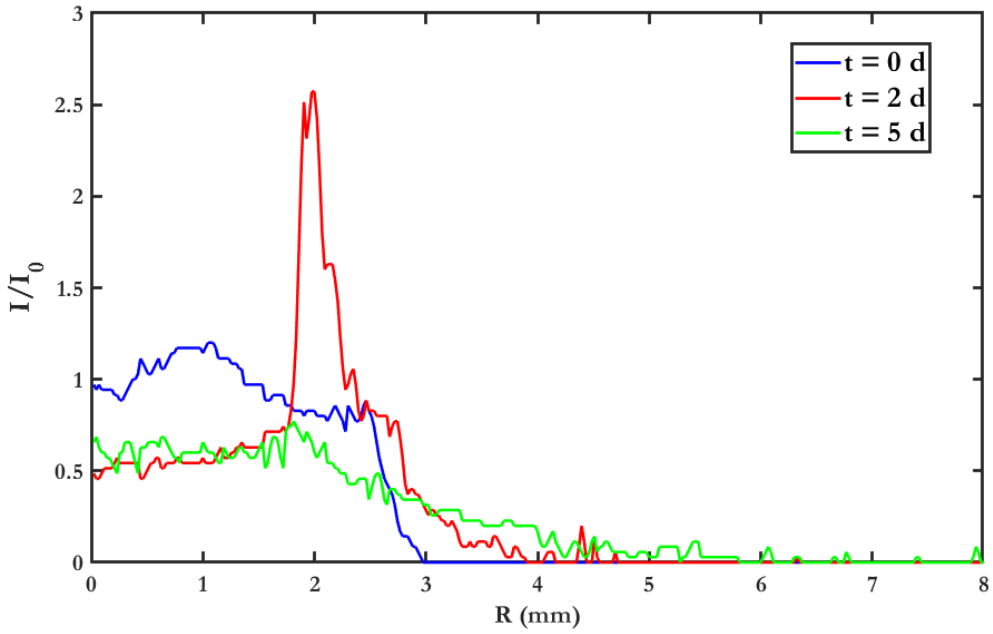

Fig. 4.8. Normalized pixel intensity distributions at three instants of time for the spreading Coomassie blue dye on 3% agar plate.

As the thickness of the agar in the petri-dish is insignificant compared to the diameter of the petri-dish (~4%), it is assumed that the dye diffusion occurs mainly on the agar surface and diffusion through the depth is comparatively negligible. Then the transport equation governing the dye diffusion can be expressed as in polar coordinates (assuming radial symmetry of spreading):

$$\frac{\partial C}{\partial t} = D\frac{\partial^2 C}{\partial R^2} \tag{4.5}$$

where $C(t,R)$ is the dye concentration and D is the diffusion coefficient of the dye (equivalent to the nutrient diffusion coefficient). The ring formation phenomenon makes it difficult to prescribe well-defined initial condition. The boundary conditions, on the other hand, are trivial (symmetry condition at $R=0$ and no flux at $R=\rho_p$). The initial condition is obtained by choosing a

mathematical function to match the dye intensity profile corresponding to the ring at, say, $t = 2$ d. The solution of the diffusion equation with this initial condition is then compared to subsequent dye intensity distributions to estimate D (and in extension, D_c). Interestingly, the estimated nutrient diffusion coefficient was found to stay nearly constant over the range of the agar concentration.

4.3.3 Colony Diffusion Coefficient

Using the estimates of the growth parameters and the nutrient diffusion coefficient, the single colony equations which were formulated in section 4.2 were solved. To estimate the diffusion coefficient of the bacterial colonies, the numerical solution of the single colony model is compared with the results from single *B. subtilis* colony experiments. The initial bacterial population density is chosen as $X_0 = 10^{-3}$ based on the initial optical density of bacterial culture in aqueous medium. The initial nutrient concentration is $c_0 = 15$ g/L which is the initial concentration of LB in the growth medium. The value of the threshold nutrient concentration c^* does not have any notable numerical consequence. In Figure 4.9, the numerical solutions for the population density X at $t = 30$ h for $D_b = 0.04 \text{ mm}^2/\text{h}$ are compared for different values of c^*. The solutions are found to change insignificantly over three orders of magnitude of c^*. Therefore, the value of c^* is chosen as 10% of c_0, $c^* = 1.5$ g/L, as was used by Patra et al. [33].

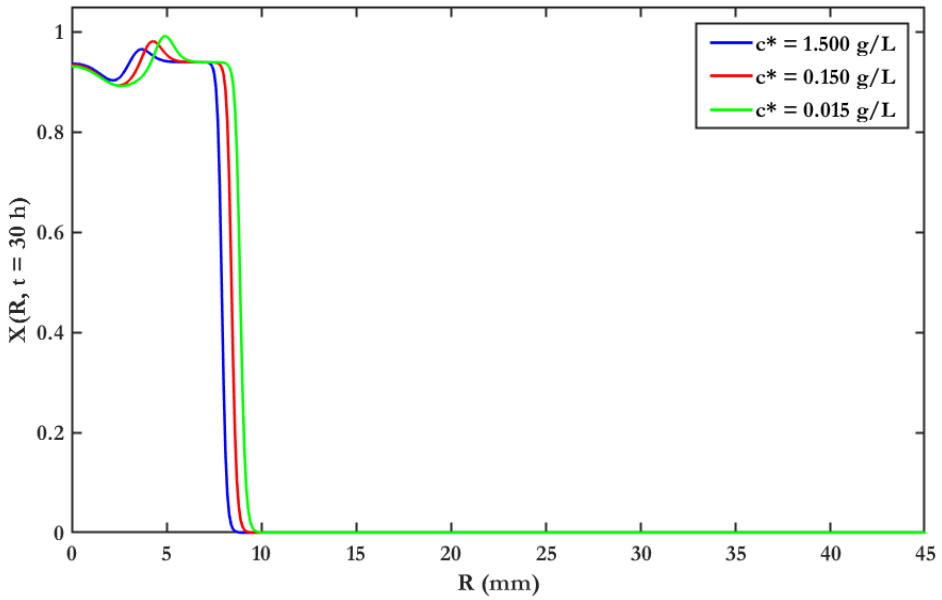

Fig. 4.9. Influence of c^* on the numerical solution of the single colony model. The solutions for the population density $X\left(R, t = 30\text{ h}\right)$ are compared for different values of c^*.

The radius of the circular domain of simulation is that of a petri-dish used in the experiments, $\rho_p = 46$ mm. The colony is inoculated at the origin in the form of a drop of radius $\rho = 2.5$ mm. As the reaction-diffusion models are essentially continuous models, it is necessary to define a reference bacterial population density X_e to demarcate the edge of the colony. This was done by matching the numerical and experimental colony diameters at t = 6 h (post incubation). As the colony diameters are nearly identical on different agar concentrations at 6 hours (Figure 4.4), consequently so is the estimate of X_e. The value of X_e was found to lie within 0.1 and 0.3. The coupled equations are spatially discretized using a second order central difference scheme. The time derivative is discretized using the Forward and Backward Euler schemes for the nutrient concentration and population density respectively. Because of radial symmetry, the governing

equations essentially reduce to an ordinary differential equation in terms of the radial coordinate R. The simulation domain is decomposed into 461 grid points, with a grid resolution of $\Delta R =$ 0.1 mm. Numerical solution is obtained between t = 0 and t = 40 hours, in steps of $\Delta t =$ 36 sec (i.e., 4001 time steps). The time step and grid resolutions were chosen after establishing grid and time step independence by comparing the numerical solution of the governing equations for different time steps and grid resolutions. Figure 4.10 illustrates the grid and time step independence of the numerical solution for the population density X at $t = 30$ h. For performing the independence tests, the following time steps and grid resolutions were chosen: $\Delta t = 36$ sec, 18 sec and 3.6 sec, and $\Delta R = 0.25$ mm, 0.1 mm and 0.05 mm. The colony diffusion coefficient for the simulation is 0.04 mm^2/h.

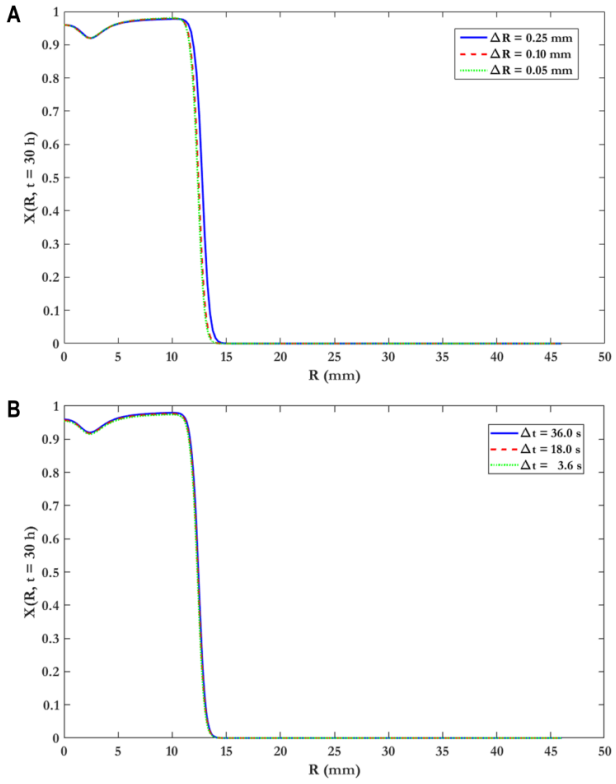

Fig. 4.10. (A) Grid and **(B)** Time step independence tests comparing the numerical solution for the population density $X(r, t = 30\ \text{h})$ for three different grid and time step resolutions.

Finally, the diffusion coefficient of the colony for the given agar concentration was estimated based on the numerical curve which best fits the experimental data. In Figure 4.11, the numerically fitted curves have been compared with the experimental data for 0.5%, 2% and 5% agar.

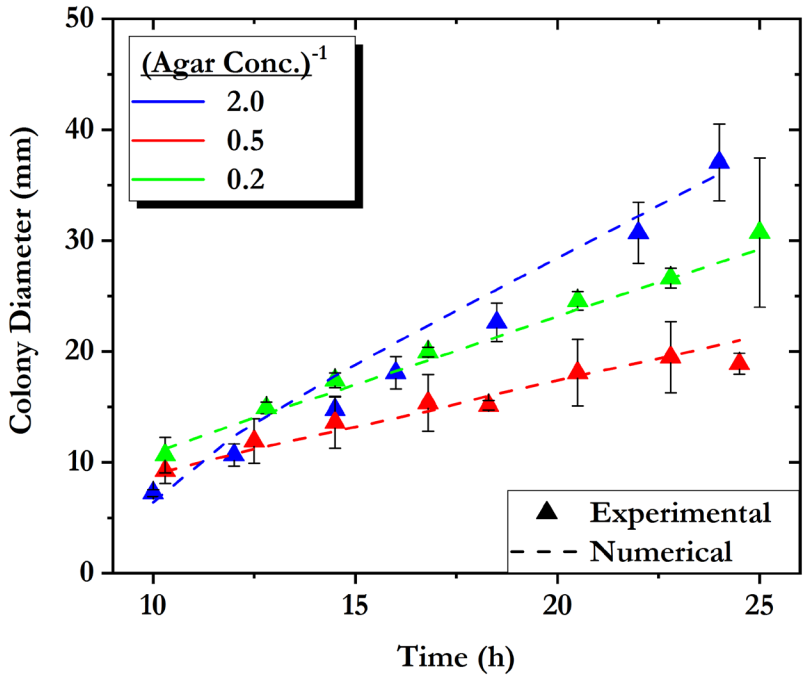

Fig. 4.11. Numerical solution of single colony model is fitted with single colony experimental data corresponding to 0.5%, 2% and 5% agar to estimate the diffusion coefficient of the colony.

By estimating D_b for different agar concentrations, the dependence of the diffusion coefficient with the agar concentration is determined which is shown in Figure 4.12. The diffusion coefficient at 0.5% agar is nearly one order of magnitude higher than the lowest estimated value which occurs at 2% agar. The diffusion coefficient decreases on increasing the agar concentration from 0.5% till 2%. Beyond 2%, interestingly, for 3% and 5% agar, there is an increase in D_b, which may be caused by excessive production of surfactin by the B. subtilis colony. The estimated data are

fitted with a polynomial function to mathematically express the correlation between D_b and the reciprocal of the agar concentration (a): $D_b = 0.05a^2 + 0.0188a^{-1}$. The quality of the fit measured in terms of the coefficient of determination is $R^2 \approx 98\%$.

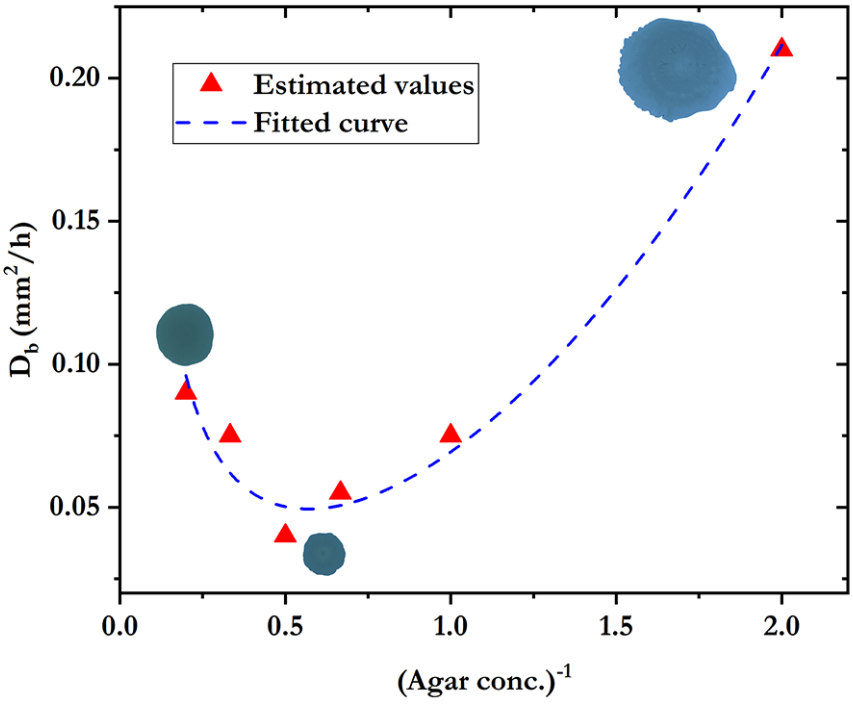

Fig. 4.12. Estimated diffusion coefficients of the colony at different agar concentrations. The insets of colonies at 0.5%, 2% and 5% agar correspond to 24 hours post inoculation.

The parameters estimated from the Monod's model and the single colony model are summarized in Table 4.1.

Table 4.1. Estimates of Model Parameters

Parameters		**Estimate**
Bacterial Growth	r_0	$4\ h^{-1}$
	γ	16 g/L
	k	42.5 g/L
Nutrient Diffusion	D_c	$10^{-3}\ mm^2/h$
Colony Dispersion	D_b	$0.04 – 0.21\ mm^2/h$

Chapter 5

Interactions Between Sibling Bacterial Colonies

Chapter 5 describes the occurrence of dual interaction patterns in *B. subtilis* colonies. The influence of physical factors on these interaction patterns is studied experimentally. A mathematical model is proposed to complement the experimental observations.

5.1 Experimental Results

5.1.1 Two Interaction Patterns in *B. subtilis*

Figure 5.1 shows examples of the two distinct interaction patterns observed under different conditions. When the concentration of agar was increased from 0.5% to 5% while keeping the separation between two sibling colonies at 20 mm, the sibling colonies change from coalescing into a single colony (Figures 5.1a), to forming an interface between the advancing colony fronts (Figure 5.1b). Similar observations were made by holding the agar concentration constant while varying the initial separation. At low agar concentrations ($<1\%$), coalescence was observed in all cases when the separation d was increased from 10 mm to 30 mm. At higher agar concentrations ($\geq 1\%$), both coalescence and interface formation were observed, with the former occurring at small colony separation (Figure 5.1c) and the latter at large colony separation (Figure 5.1b). It is interesting to note that the morphology of the colonies vary as the concentration of agar is increased from 0.5% to 5%. The colonies growing on 0.5% are nearly circular and the boundaries of the colony appear to be smooth. This is distinctly different from the colonies on 2% and 5% agar where the edges of the colonies are jagged assuming a viscous fingering like appearance after a long post-inoculation time.

The colonies are also found to develop wrinkles over time. The variation in the morphology can be attributed to both genetic as well as environmental factors. Inside the colony, bacterial cells are continuously undergoing genetic mutations, which allow cells in each generation to take on characteristics slightly different from its parents [86, 87]. Over multiple cycles of proliferation, these differences may become quite distinct from the original cells. One of such differences is that of flagellar motility. In certain conditions cells in different parts of the colony mutate and acquire different flagellar motilities. Hence, the colony boundaries progress at different rates at different locations, giving rise to a viscous fingering like appearance. The colony growing on 0.5% agar spreads very fast and as a result, it is difficult to spot the changes in flagellar motility brought about by mutations. This, however, is clearly visible on 2% and 5% agar, where colonies progress slowly. The wrinkling in colonies, on the other hand, is brought about by environmental factors as an adaptive feature which enables bacteria to survive in nutrient deficient environments [88]. As the colonies grow, the central regions of the colonies are deprived of water and nutrients as bulk of these resources are consumed by cells at the periphery. In order to supply nutrition deep inside the colony, narrow micro-channels are formed which run radially from the centre of the colony towards the periphery. Water and nutrients are transported through these veins from the periphery towards the center. These micro-irrigation channels cause the colony to appear wrinkled [88]. On 0.5% agar, bacterial colonies spread rapidly and cells are able to procure nutrition easily compared to colonies growing on 2% and 5% agar. Hence, wrinkles do not appear on 0.5% agar, but this feature is abundant on colonies growing in more unfavourable environments such as on 2% and 5% agar.

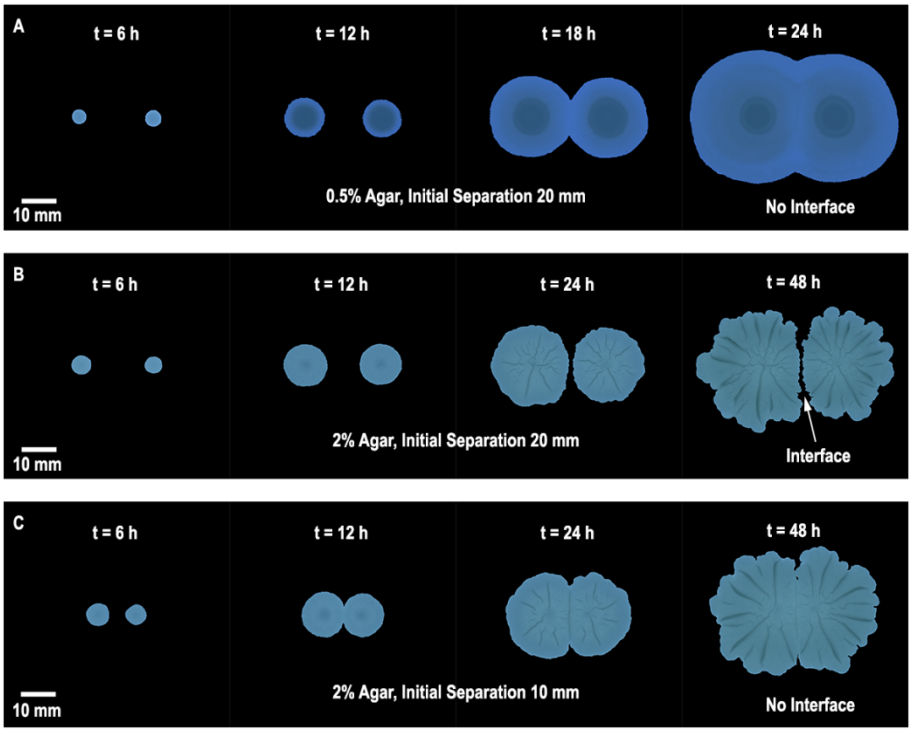

Fig. 5.1. Time lapse images of interacting *B. subtilis* colonies. **(A)** Colonies separated by 20 mm growing on 0.5% agar growth medium coalesce without forming an interface. **(B)** With the same initial separation, on 2% agar, the colonies are seen to form a distinct interface. **(C)** When the colonies are brought closer at $d =$ 10 mm on 2% agar, no interface is observed**.**

By systematically varying the agar concentration and the colony separation, a phase diagram is generated to document the conditions in which each of the two interactions occurs. Figure 5.2 shows the phase diagram depicting the interaction regimes in *B. subtilis*. The phase diagram shows the existence of two distinct domains depending on the agar concentration and the separation between the colonies.

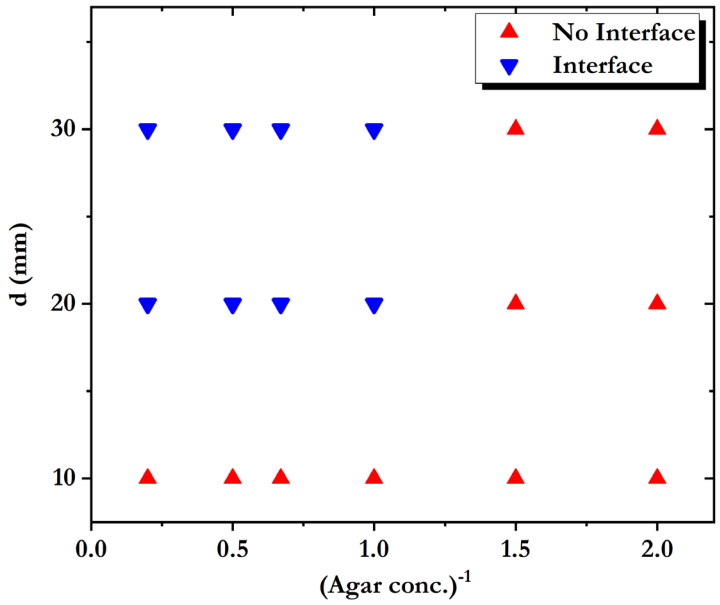

Fig. 5.2. Experimentally obtained phase diagram showing the two interaction regimes in *B. subtilis*: Coalescence (red) and Interface formation (blue).

5.1.2 Interaction with Physical Objects

The advancing fronts of sibling colonies are physical obstacles in the progression of the colonies. It is possible that the sibling colonies act as mutual physical deterrence and prevent coalescence in high agar concentrations and/or when the colonies are relatively far apart. To see if interface formation is induced by the presence of physical barriers, one of the colonies was simulated with a physical object (liquid: castor oil droplet or a solid structure: PDMS and PP walls and discs) and let a *B. subtilis* colony grow adjacent to the physical object. PDMS and PP are commonly used solid substrates in bacteriological studies and are known to be compatible with bacterial growth [89-93]. The solid PDMS and PP structures were created in the form of a flat wall (to simulate a flat interface formed between sibling colonies as in Figure 5.1b) and a circular disc (to represent a growing colony). Figure 5.3 shows how the *B. subtilis* colonies interact with these physical

obstacles. In all cases, it is observed that the colonies growing along the edge of the physical structures showing no signs of interface formation. The separations between the colonies and the physical barriers have been so chosen that at these separations, interface formation has been observed in two colony experiments but is absent here. The experiments clearly show that the presence of a physical deterrence may not, by itself, lead to an interface being formed. Only when a sibling colony is present in the vicinity does an interface form under the appropriate combination of agar concentration and separation. This suggests that interface formation is not primarily dictated by physical factors, but rather by biochemical inhibition due to the presence of a sibling colony.

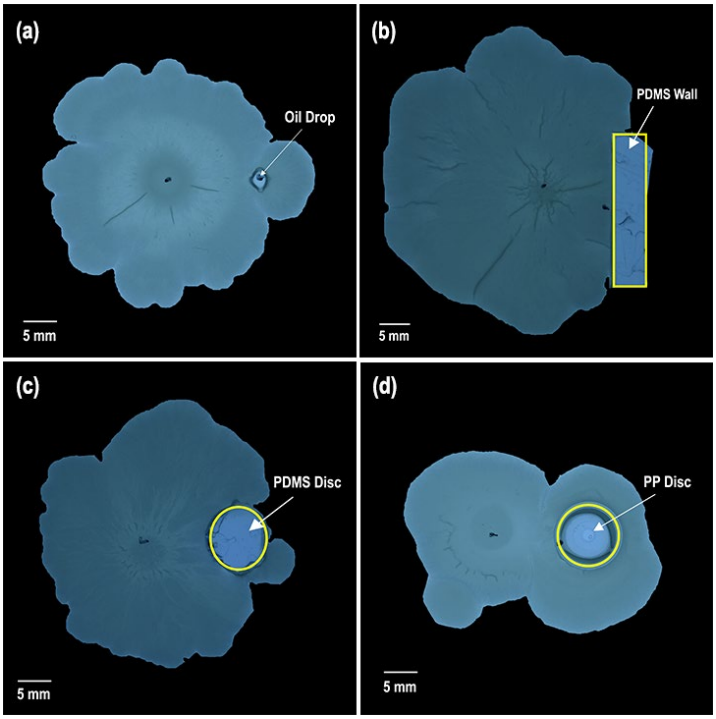

Fig. 5.3. Interaction of *B. subtilis* colonies with liquid and solid substrates produces no interfaces under similar conditions. **(a)** Colony interacting with sessile castor oil droplet. The colony grows around the oil droplet without any interface formation. Image corresponds to 78 hours post inoculation. **(b)** Approaching sibling colony front is simulated with a solid PDMS wall. The colony grows till the edge of the solid wall but do not form any interface near the flat solid surface of the wall. Image was taken 48 hours after inoculation. **(c)** A PDMS disc is used as a simulacrum for a sibling colony. In this case also, the colony does not form an interface but grows around the solid disc. Image was taken 48

hours after inoculation. **(d)** Like the PDMS disc, the colony reaches and grows around a PP disc. Image was taken 28 hours after inoculation. All four experiments were performed on 1.5% agar media.

5.2 Mathematical Model

A two-colony model is formulated as an extension of the single colony model and a mortality term is incorporated which accounts for the interaction between the sibling colonies. Mathematically, the two-colony model is expressed as:

$$\begin{aligned}
\frac{\partial X_1}{\partial t} &= r(c)X_1 + \nabla\cdot\left(D_b\mathcal{H}\left[c-c^*\right]\nabla X_1\right) - m(t) \\
\frac{\partial X_2}{\partial t} &= r(c)X_2 + \nabla\cdot\left(D_b\mathcal{H}\left[c-c^*\right]\nabla X_2\right) - m(t) \\
\frac{\partial c}{\partial t} &= -\gamma r(c)X + \nabla\cdot\left(D_c\nabla c\right)
\end{aligned} \tag{5.1}$$

In this model, the two colonies are assumed to be identical to each other, and hence the same model parameters, including Monod's growth parameters and diffusion coefficients will be used for both colonies. Furthermore, it is also assumed that these parameters will be the same as those for a single colony, i.e., growth characteristics are unaffected because of inter-colony interactions. Unlike the single colony model, the two-colony model is defined in the Cartesian coordinate system as radial symmetry is absent in this case. $X_1(t,x,y)$ and $X_2(t,x,y)$ are the population densities of the two colonies, $m(t)$ is the mortality rate. $X = X_1 + X_2$ is the net population density. The two colonies are inoculated symmetrically on each side of the origin on the x axis in the form of sessile drops as described in chapter 4. Figure 5.4 shows the domain of simulation at $t = 0$. All other variables and parameters have been previously defined. In order to fully describe the two-colony system, the mortality rate must be formulated based on experimental results.

The biochemical inhibition has been shown to cause cell death at the advancing fronts of the sibling colonies thereby being responsible for the interface formation. To model this cell mortality, the mortality rate $m(t)$ has been assumed to be proportional to the population densities of each of the sibling colonies, i.e., $m(t) = \mu X_1 X_2$, where the mortality coefficient μ is the constant of proportionality. Defining $m(t)$ in this fashion is advantageous in some ways. At the initial stages of the colony spreading, $m(t)$ is zero everywhere and the colonies grow independently without any inhibition. This is consistent with experiments. As the colony starts interacting with each other, $m(t)$ becomes active near the advancing fronts of the two colonies. Elsewhere, it is zero. By using this definition of $m(t)$ one can numerically generate an interface between the colonies, as has been demonstrated by Patra et al. [33]. But the drawback of this formulation is that the mortality term always produces an interface and the colonies cannot coalesce, which is not consistent with the experimental results. To address this issue, the transport of inhibition factors which are produced by the sibling colonies in response to the advancing colony was examined. The investigation of Be'er et al. showed that these inhibition factors have high molecular weight (on the order of 10^4 g/mol) and they inhibit colony spreading only when the concentration is higher than a lethal value. Owing to the high molecular mass of these factors, they diffuse through the agar medium very slowly and cause inhibition only after some critical time. Experiments in this work have shown that when two colonies exhibit coalescence, the two colonies start merging with each other at around 20 hours post inoculation (or earlier). On the other hand, when there is an interface formation, the two colonies start interacting at around 24 hours. It is therefore assumed that the effect of the biochemical inhibition occurs sometime after 20 hours. Based on this assumption, the effect of the inhibition factors has been incorporated by defining a critical time t^*. For $t < t^*$ inter-colony inhibition is

absent, i.e., $m(t)=0$ and for $t>t^*$, a non-zero $m(t)$ leads to interface formation. This is done by using the Heaviside step function to augment $m(t)$, i.e. $m(t)=\mu X_1 X_2 \mathcal{H}\left[t-t^*\right]$. Based on experimental observations, $t^*=20$ h is chosen, although physical meaning of this value is yet to be investigated. The new mortality function can produce coalescence and interface depending on the values of d and D_b. But the coalescence in this case is unstable and the coalesced colonies separate again for $t>t^*$ when $m(t)$ becomes active. This is not physically observed in experiments. Instead, the colonies which coalesce continue to grow together as a single unit henceforth. This may be because after colonies coalesce, mutual inhibition is arrested, and two colonies become part of a single community. This condition has been imposed by introducing a second Heaviside step function which ensures that the mortality rate remains inactive after colonies coalesce. The final form of the mortality rate $m(t)$ is expressed as follows:

$$m(t)=\mu X_1 X_2 \mathcal{H}\left[t-t^*\right]\mathcal{H}\left[X_e - X\left(t,x=0,y=0\right)\right] \tag{5.2}$$

$X\left(t,x=0,y=0\right)$ is the net population density midway between the centers of two colonies located at the coordinates $x=0, y=0$ (see Figure 5.4). X_e is a cut-off population density which demarcates the edge of each colony. It is to be noted that the mortality rate is a function of both time and space coordinates. Spatially, its effect is felt only at the midway between the two colonies where the interface forms, while the temporal dependence of the function is of key importance. Hence, for the sake of simpler notation, the space dependence has been omitted and the mortality rate is denoted simply by $m(t)$.

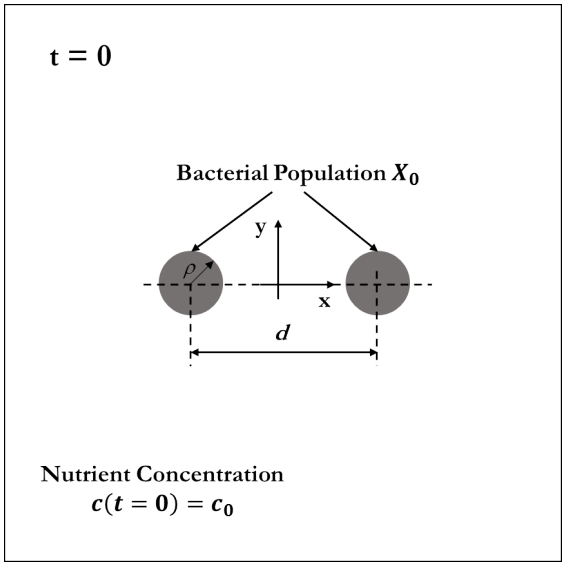

Fig. 5.4. Schematic showing the domain of numerical simulation at t = 0. The bacterial colonies are inoculated in the form of sessile drops of radius ρ (in grey) with initial bacterial population X_0. The initial nutrient concentration c_0 in the growth medium is uniform. The separation between the inoculated colonies is d.

The established RD equations, equation (5.1) along with (5.2), are solved with appropriate initial and boundary conditions. At t = 0, when the nutrient concentration in the medium is homogenous and the colonies are inoculated as sessile droplets of radius ρ at y = 0 symmetrically about the origin with a center-to-center separation of d (Figure 5.4), i.e.,

$$X_1\left(t=0,\left(x-\frac{d}{2}\right)^2+y^2\le\rho^2\right)=X_2\left(t=0,\left(x+\frac{d}{2}\right)^2+y^2\le\rho^2\right)=X_0$$
$$c\left(t=0,x,y\right)=c_0. \tag{5.3}$$

The simulation domain is a $2\rho_p\times 2\rho_p$ square (ρ_p is the radius of petri-dish). At the boundary (Γ) of the domain, no flux boundary condition is enforced for the population densities and a constant nutrient concentration c_0 is assumed as in the case of the single colony model:

$$\nabla X_1 \cdot \hat{\mathbf{n}}\big|_\Gamma = \nabla X_2 \cdot \hat{\mathbf{n}}\big|_\Gamma = 0$$
$$c\big|_\Gamma = c_0 \tag{5.4}$$

The equations and corresponding initial and boundary conditions is non-dimensionalized so that the results can be applicable to a broader range of bacterial systems. For non-dimensionalization, r_0^{-1} and $\sqrt{D_c/r_0}$ are used as the time and length scales in the non-dimensionalization and the corresponding dimensionless variables are defined as follows:

$$\tau = r_0 t, \tau^* = r_0 t^* \tag{5.5}$$

$$\bar{\rho} = \sqrt{\frac{r_0}{D_c}}\rho, \bar{\nabla} = \sqrt{\frac{D_c}{r_0}}\nabla, \bar{\rho}_0 = \sqrt{\frac{r_0}{D_c}}\rho_0, \bar{\rho}_p = \sqrt{\frac{r_0}{D_c}}\rho_p, \bar{d} = \sqrt{\frac{r_0}{D_c}}d \tag{5.6}$$

The dependent variables and parameters related to the population density and the nutrient concentrations are non-dimensionalized in terms of the initial condition as follows:

$$\bar{X}_1 = \frac{X_1}{X_0}, \bar{X}_2 = \frac{X_2}{X_0}, \bar{c} = \frac{c}{c_0}, \bar{c}^* = \frac{c^*}{c_0}, \bar{k} = \frac{k}{c_0}, \bar{\gamma} = \gamma\frac{X_0}{c_0}, \bar{\mu} = \mu\frac{X_0}{r_0} \tag{5.7}$$

The normalized diffusion coefficient $\bar{D}$ is defined as $\bar{D} = D_b/D_c$.

The dimensionless set of governing equations with initial and boundary conditions are as follows:

Governing equations

$$\begin{aligned}
\frac{\partial \overline{X}_1}{\partial \tau} &= \overline{r}\left(\overline{c}\right)\overline{X}_1 + \overline{\nabla}\cdot\left(\overline{D}\mathcal{H}\left[\overline{c}-\overline{c}^*\right]\overline{\nabla}\overline{X}_1\right) - \overline{m}\left(\tau\right) \\
\frac{\partial \overline{X}_2}{\partial \tau} &= \overline{r}\left(\overline{c}\right)\overline{X}_2 + \overline{\nabla}\cdot\left(\overline{D}\mathcal{H}\left[\overline{c}-\overline{c}^*\right]\overline{\nabla}\overline{X}_2\right) - \overline{m}\left(\tau\right) \\
\frac{\partial \overline{c}}{\partial \tau} &= -\overline{\gamma r}\left(\overline{c}\right)\overline{X} + \overline{\nabla}\cdot\left(\overline{\nabla}\overline{c}\right) \\
\overline{m}\left(\tau\right) &= \overline{\mu}\overline{X}_1\overline{X}_2\mathcal{H}\left[\tau-\tau^*\right]\mathcal{H}\left[\overline{X}^{\Gamma} - \overline{X}\left(\tau,\overline{x}=0,\overline{y}=0\right)\right]
\end{aligned} \tag{5.8}$$

Initial conditions

$$\begin{gathered}
\overline{X}_1\left(\tau=0,\left(\overline{x}-\frac{\overline{d}}{2}\right)^2+\overline{y}^2\le\overline{\rho}^2\right) = \overline{X}_2\left(\tau=0,\left(\overline{x}+\frac{\overline{d}}{2}\right)^2+\overline{y}^2\le\overline{\rho}^2\right) = 1 \\
\overline{c}\left(\tau=0,\overline{x},\overline{y}\right)=1
\end{gathered} \tag{5.9}$$

Boundary conditions

$$\begin{gathered}
\overline{\nabla}\overline{X}_1\cdot\hat{\mathbf{n}}\big|_{\overline{\Gamma}} = \overline{\nabla}\overline{X}_2\cdot\hat{\mathbf{n}}\big|_{\overline{\Gamma}} = 0 \\
\overline{c}\big|_{\overline{\Gamma}} = 1
\end{gathered} \tag{5.10}$$

5.3 Numerical Results and Comparison with Experiments

The growth parameters, the diffusion coefficients and the reference time t^* depend on the bacterial species, composition of the nutrient and the experimental conditions which include the agar concentration and the bacterial biomass in the inoculum. As a result, these parameters are to be determined experimentally to be used in the mathematical model. The other model parameters are chosen on the basis of experimental design and numerical stability within bounds of tenable physical significance. In chapter 4, the growth parameters and the diffusion coefficients of the nutrient and the colony have been estimated which are used in solving the two-colony model. The variation of D_b with agar (Figure 4.12) is necessary to study how agar influences colony interactions from a

numerical viewpoint. The initial conditions for the population density of each colony and the nutrient are identical to the single colony model, $X_0 = 10^{-3}, c_0 = 15\,\text{g/L}$. Based on experimental observation, $t^* = 20\,\text{h}$. The reference population X_e is chosen based on experimental results discussed in chapter 4 as $X_e = 0.3$. The coefficient of mortality μ is a theoretical parameter defined in order to numerically generate a stable interface by incorporating the inhibitory interaction between colonies. As there is no direct way of estimating the value of μ experimentally, a parametric analysis of μ was conducted numerically. In Figure 5.5 the numerical solutions for the population density X at $t = 30\,\text{h}$ taken along the x axis ($y = 0$) are compared for $\mu = 4/\text{h}\left(\bar{\mu} = 10^{-3}\right)$, $\mu = 40/\text{h}\left(\bar{\mu} = 10^{-2}\right)$ and $\mu = 400/\text{h}\left(\bar{\mu} = 10^{-1}\right)$. For the simulation, $D_b = 0.04\ \text{mm}^2/\text{h}$ and the colony boundary is demarcated by the threshold population density $X_e = 0.3$. For very small values of μ, e.g., $\mu = 4/\text{h}\left(\bar{\mu} = 10^{-3}\right)$, the numerical solution demonstrates that there is no interface generated because the mortality term is negligible. At larger values of μ, $O\left(10^{-2}\right) \le \bar{\mu} \le O\left(10^{-1}\right)$, interfaces can be observed and the results are insensitive to the specific values of μ. Very large values of μ, on the other hand, makes the solution numerically unstable. From the results of the parametric study, μ is chosen to be $\mu = 40/\text{h}$.

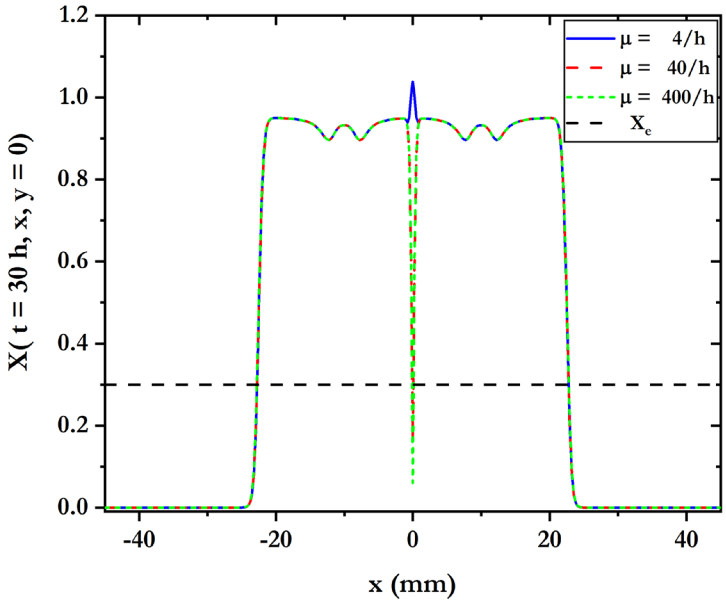

Fig. 5.5. Influence of μ on the numerical solution. The solutions for the population density $X\left(t = 30\text{ h}, x, y = 0\right)$ are compared for different values of μ.

Other model parameters including c^*, ρ and the domain size are identical to those used in the single colony model. The coupled equations are solved using the second order Forward-Time Central-Space (FTCS) scheme. The rectangular simulation domain is decomposed into 369 x 369 grid points, with a grid resolution of $\Delta x = \Delta y =$ 0.25 mm. Numerical solution is obtained between t = 0 and t = 48 hours, in steps of $\Delta t =$ 34 sec (i.e., 5001 time steps). The time step and grid resolutions were chosen after establishing grid and time step independence by comparing the numerical solution of the governing equations for different time steps and grid resolutions. Figure 5.6 illustrates the grid and time step independence of the numerical solution for the population density X at $t = 30\,\text{h}$ along the x axis $\left(y = 0\right)$. The colony separation is 20 mm and colony diffusion coefficient is 0.04 mm^2/h. For performing the independence tests, the following time steps

and grid resolutions were chosen: $\Delta t = 68$ sec, 34 sec and 17 sec, and $\Delta x = \Delta y = 0.25$ mm, 0.1 mm and 0.05 mm.

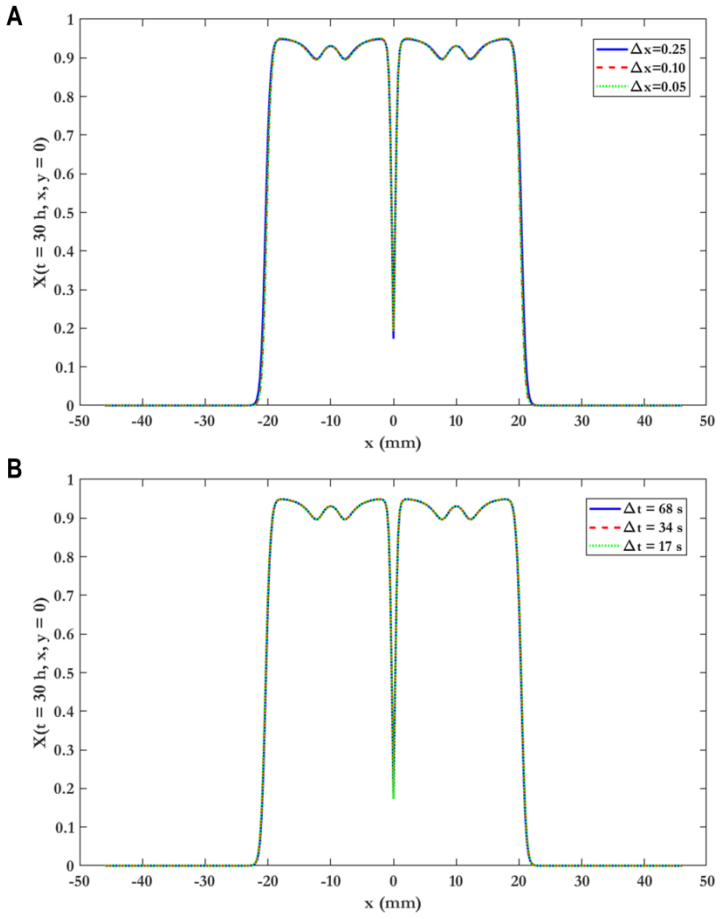

Fig. 5.6. Independence tests on numerical solution: **(A)** Grid and **(B)** Time step independence tests comparing the numerical solution for the population density $X\left(t = 30 \text{ h}, x, y = 0\right)$ for three different grid and time step resolutions.

The numerically simulated colony interactions are shown in Figure 5.7 for different values of the diffusion coefficient D_b and the initial separation d. The morphology of the numerically generated colony is defined by the reference population X_e which is predefined. Hence, the numerical solution objectively determines coalescence or interface formation. Figure 5.7a shows that

colonies coalesce when the diffusion coefficient is 0.21 mm^2/h and the initial separation is 20 mm. The diffusion coefficient, in this case, is large and corresponds to very low agar concentrations (~0.5%) when bacteria are highly motile and the colonies spread rapidly. Experimentally, the conditions represent those in Figure 5.1a. When the diffusion coefficient is reduced by almost one order of magnitude to 0.04 mm^2/h without changing the initial separation (Figure 5.7b), an interface forms. This case depicts Figure 5.1b at 48 h. Finally, in Figure 5.7c, the initial separation is reduced to 10 mm while keeping the diffusion coefficient constant. Here, the colonies coalesce completely without any interface formation, as seen in Figure 5.1c. Therefore, there is a good qualitative agreement between the experiments and the proposed mathematical model.

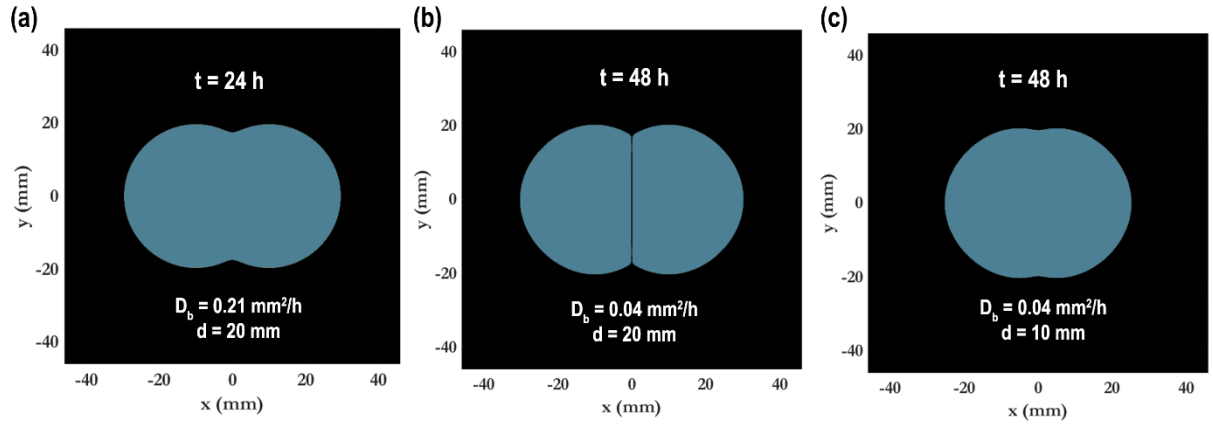

Fig. 5.7. Numerical simulation of *B. subtilis* colonies. **(A)** No interface is formed when the diffusion coefficient is large. Here $D_b = 0.21\ \mathrm{mm}^2/\mathrm{h}$ and initial separation d = 20 mm. **(B)** Interface forms when the diffusion coefficient is reduced to $0.04\ \mathrm{mm}^2/\mathrm{h}$ while holding d constant. **(C)** If, however, d is lowered to 10 mm without changing the diffusion coefficient, coalescence occurs.

Figure 5.8a shows a dimensionless phase diagram in the $\overline{d} - \overline{D}$ space where two distinct regimes underline the generalized conditions for whether two colonies would form an interface or coalesce. To determine whether the colonies coalesce or form an interface numerically, the total

population density midway between the centers of two colonies is checked at an instant when $t > t^*$. If $X\left(t > t^*, x = 0, y = 0\right) \geq X_e$, there is a coalescence, else an interface forms. For each value of $\bar{D}$, there exists a critical separation $\bar{d}^*$, where the nature of interaction changes from coalescence to interface. $\bar{d}^* = f\left(\bar{D}\right)$ determines the boundary between the coalescence and interface regimes in the phase diagram. The function *f* can be well approximated as a power law relation $\bar{d}^* = \alpha \bar{D}^n$, where α and n are numerical constants. α and n has been found numerically as: $\alpha = 276.55, n = 0.377$. From this simple empirical expression, it is possible to predict, with an acceptable degree of accuracy, the outcome of interaction between two sibling colonies given the initial separation and the diffusion coefficient (in extension, the agar concentration). Using the estimated parameter values, the corresponding dimensional phase diagram is plotted in Figure 5.8b, which shows that when the separation is sufficiently small e.g., $d \leq 10$ mm, the sibling colonies would coalesce irrespective of the value of the agar concentration. The model also predicts that when the agar concentration is very low, the colonies coalesce even when the separation is as high as 30 mm. These predictions are in good agreement with the experimental findings. In Figure 5.8, the phase boundary demarcates the regions where the behavior of colonies changes from being "family" to "enemy". Therefore, we will refer to the phase boundary denoted by the power law relation as the "*Laxman Line*" (based on the *Laxman Rekha* described in the Indian epic, the Ramayana).

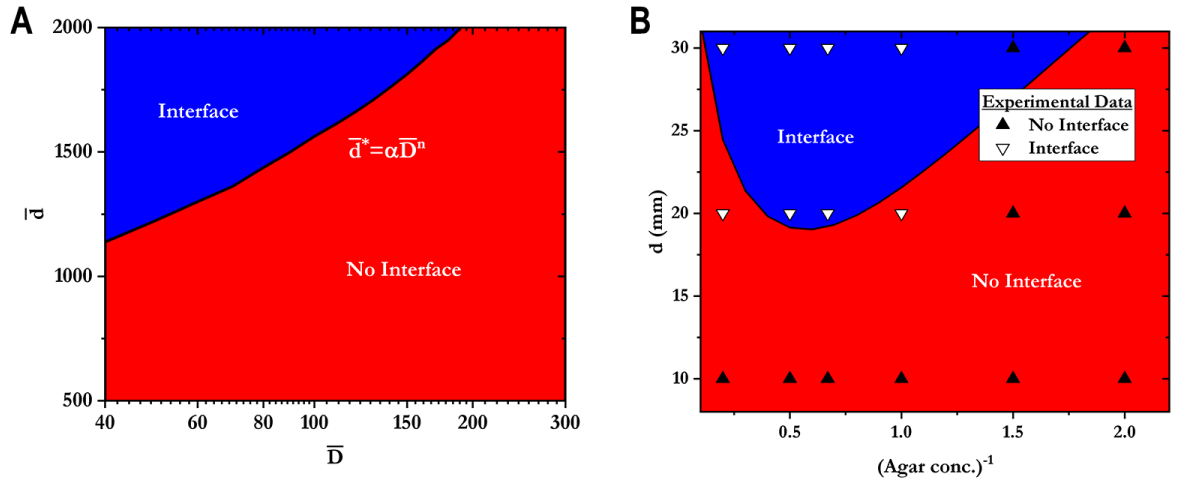

Fig. 5.8. Numerical phase plots for interface formation in *B. subtilis* colonies. **(A)** Phase plot showing interface formation in a dimensionless variable space. **(B)** Experimental phase diagram superposed on the dimensional numerical phase plot for estimated parameters r_0 = 4/h and D_c = 0.001 mm^2/h.

The exponent n in the empirical relation $\bar{d}^* = \alpha \bar{D}^n$ has some interesting implications. Figure 5.9 plots $\bar{d}^*$ against $\bar{D}$ for different values of the exponent, while keeping the coefficient $\alpha = 276.55$ as constant. On increasing the value of n from 0.377 to 0.5, the boundary line separating the two phases becomes steeper and $\bar{d}^*$ increases for the same $\bar{D}$. This means that the sibling colonies would be more susceptible to coalescence. On the other hand, on decreasing n from 0.377 to 0.2, the boundary line becomes flatter and shifts downwards, which signifies that the colonies would tend to form interfaces. Physically, one can expect n to be large in bacterial species which are known to coalesce such as identical strains of *P. mirabilis*. Bacterial species such as *P. dendritiformis* tend to form an interface between sibling colonies when they interact. For such species, one can expect the exponent n to be small.

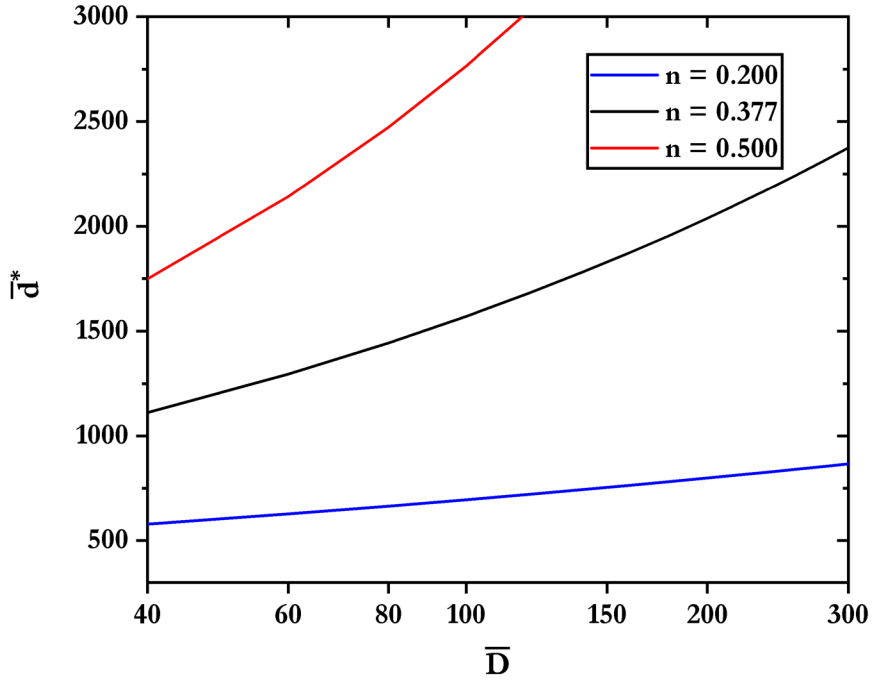

Fig. 5.9. Effect of the empirical index n on the critical dimensionless separation $\overline{d}^*$. $n = 0.377$ represents the numerical estimate. On the dimensionless phase diagram, for higher n, inter-colony interaction is dominated by coalescence, whereas for lower values, the interaction is interface dominated.

5.4 Discussions

The present experiments have shown that the concentration of agar influences the rate of spreading of *B. subtilis* colonies. In chapter 4, it has been shown that at low concentrations ($<1\%$), bacteria can swarm rapidly on the surface and derive nutrition from the growth medium. As the concentration of agar is increased, colonies spread slowly. On 0.5% agar, due to rapid swarming, the colonies experience less competition in procuring nutrient and consequently are found to coalesce with sibling colonies even when the initial separation is as large as 30 mm. This is, however, not true for higher agar concentrations. The unfavourable condition of the growth medium may trigger

biochemical inhibition as a defense mechanism and thereby lead to interface formation when the separation is 20 mm or higher.

The duality of interface and coalescence is not specific to *B. subtilis*. While *B. subtilis* is a Gram-positive bacterium, experiments with Gram-negative *Pseudomonas fluorescens* showed that this phenomenon is a general one exhibited by multiple species of bacteria (see Figures 5.10a for examples). Figure 5.10 also helps depict that the formation of interface between sibling bacterial colonies is not confined to the previously or currently reported species, but most likely a very generic biophysical phenomenon.

Several comments are made regarding the underlying assumptions and the limitation of the proposed mathematical model. The RD model proposed in this work is based on the assumption that biochemical inhibition is brought about by inhibitor factors which have very large molecular mass (on the order of 10^4 g/mol). Because of their high molecular mass, these factors diffuse very slowly through the agar medium and cause cell death in the approaching colony when a lethal concentration is reached. The present work did not investigate the presence of these inhibition factors or explicitly account for their diffusion. Instead, their effect has been incorporated by using a reference time t^* in the model. This limitation can be removed by explicitly solving the transport equation of the biochemical inhibition factors. An attempt has been made to formulate a generalized mathematical model to describe the dual interaction patterns that may be applicable to multiple species of bacteria (e.g. *P. fluorescens*). For this reason, no comments have been made on the underlying biochemical processes that lead to interface formation specific to *B. subtilis* (e.g. sporulation). An order of magnitude estimate of the nutrient diffusion coefficient has been used and assumed it to be constant. In reality, however, the diffusion coefficient of the nutrient can be expected to vary with agar concentration.

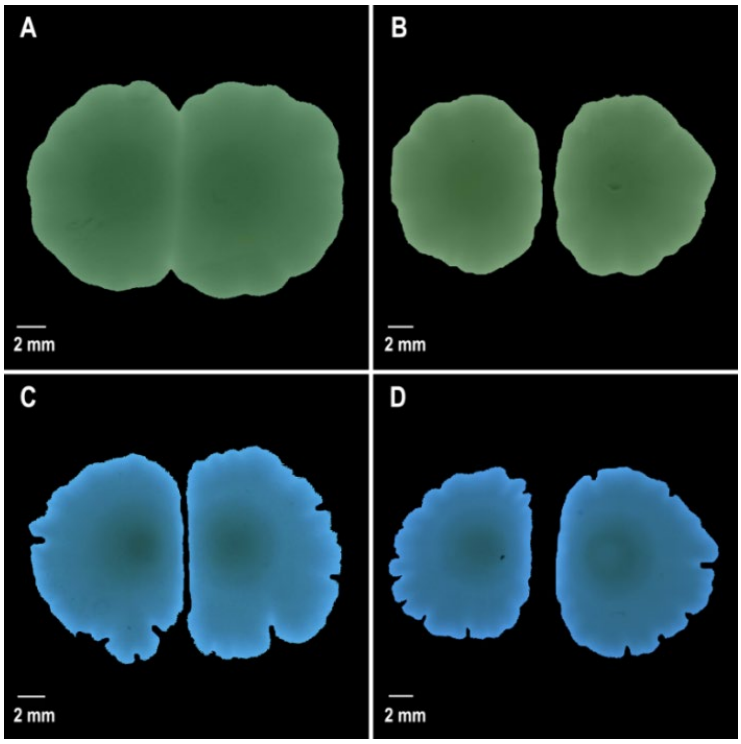

Fig. 5.10. Interaction patterns in *P. fluorescens* (**A** and **B**) and *E. coli* (**C** and **D**) on 1.5% and 0.5% agar media respectively. **(A)** Coalescence occurs in *P. fluorescens* when the $d = 5$ mm. **(B)** Interface forms when $d = 10$ mm. **(C)** In *E. coli* an interface forms when d = 5 mm. **(D)** An interface also forms when $d = 10$ mm. But in this case the gap between the interacting colony fronts is significant. All images are taken 7 days post incubation.

Chapter 6
Conclusions and Future Work

In this thesis, the influence of physical factors in the inter-colony interactions in *B. subtilis* has been investigated by varying the agar concentration in nutrient rich growth media and the initial separation between the colonies. Depending on the combination of these parameters, the colonies either coalesce or form an interface. To the best of our knowledge, this is the first evidence of two sibling colonies forming two distinct interaction patterns regulated by the agar concentration and the separation between colonies. From interactions in sibling *P. fluorescens* colonies, it has been found that these dual interaction patterns constitute a general behavior in certain bacteria. A *B. subtilis* colony has been found to form an interface only when an adjacent sibling colony is present, and not when a physical obstacle is present in the vicinity of the colony. This indicates that the interface formation is brought about by biochemical inhibition due to the colonies and is not influenced by presence of any physical deterrence. But the biochemical inhibition between sibling colonies have been found to be governed by the agar concentration which affects the radial spreading of the colonies, and the separation between the colonies which qualitatively indicates the maturity of the interacting colonies.

Based on the experimental observations, a reaction-diffusion model has been formulated to reproduce the interaction patterns in *B. subtilis*. Monod's nutrient depletion model has been used to describe the transport and consumption of nutrients. A time dependent mortality rate has been defined which can numerically generate both interactions: coalescence and interface formation using the same model, possibly the only existing mathematical model to do so. The effect of agar has been

incorporated into the model in terms of the diffusion coefficient of the bacterial colony. The model implicitly considers the diffusion of inhibition factors as a part of the mortality term. The uniqueness of the model lies in the dimensionless solution of the governing equations which makes the solution versatile and can be extended to different bacterial systems. The model generates a numerical phase diagram which separates the two interaction regimes in terms of the dimensionless separation $\bar{d}$ and the ratio of diffusion coefficients $\bar{D}$. The numerical and experimental phase diagrams have been found to be in good agreement. The dimensionless critical separation $\bar{d}^*$ which demarcates the two regimes follows a simple power law relation, $\bar{d}^* = \alpha \bar{D}^n$ which allows one to predict the nature of interaction for a given combination of the parameters. The exponent *n* is physically significant. On the dimensionless phase diagram large values of *n* correspond to bacterial species which tend to coalesce when they interact, for instance in identical strains of *P. mirabilis*, and for smaller values of *n* the bacterial colonies form interface when they interact as in *P. dendritiformis* and *E. coli*.

The interaction between multiple bacterial colonies is a poorly understood phenomenon with a dearth of scientific literature on this topic, especially from a biophysical standpoint. Hence, there exists a lot of open questions which need to be addressed. To further our understanding of the physical processes that influence this phenomenon, it is necessary to investigate the individual effects of osmotic pressure and presence of biosurfactants which are known to influence growth and spreading of bacterial colonies. The role of osmotic pressure could be illustrated by comparing the interaction phase diagram of a matrix forming strain of *B. subtilis* (such as the one used in the present study) with a non-matrix producing strain of the same bacteria. In addition, the concentration of nutrients could be used as a parameter to modulate the osmotic pressure between the bacterial soft matter and the growth medium. To test the influence of surface tension on the nature of colony interactions, one might consider using two different strains of *B. subtilis*: one which naturally produces the biosurfactant surfactin, and the other a mutant strain which is incapable of producing

surfactin. The objective will be to find out how inter-colony interaction dynamics is altered for each of these strains. An artificial surfactant such as Tween 20 may also be used to further elucidate the role of surface tension. In terms of mathematical modelling, there do not exist any hydrodynamic models to numerically simulate the two interaction patterns. It would be an interesting exercise to model the biochemical inhibition between two bacterial colonies, and subsequently reproduce the experimental results numerically. Further, to quantitatively study the effects of osmotic pressure and surface tension, a hydrodynamic model will be essential as RD models would have limited use in such applications.

In conclusion, the current experimental study reports a general inter-colony interaction phenomenon where sibling colonies exhibit both coalescence and interface formation depending on certain physical factors. The proposed mathematical model provides a good qualitative and quantitative representation of the phenomenon. The experimental study and the mathematical model provide useful insights into the dynamics of colony interactions and show that both biochemical and physical factors together control inter-colony interactions. Many features of multi-colony interaction remain ill-understood. A few directions for future research have been suggested both from an experimental and a numerical point of view which will enhance the understanding of different biophysical processes that dictate how colonies interact with each other.

List of References

[1] J. A. Shapiro, "Bacteria as Multicellular Organisms," *Scientific American,* vol. 258, no. 6, pp. 82-89, Jun 1988.

[2] E. Ben-Jacob, O. Schochet, A. Tenenbaum, I. Cohen, A. Czirok, and T. Vicsek, "Generic Modeling of Cooperative Growth-Patterns in Bacterial Colonies," *Nature,* vol. 368, no. 6466, pp. 46-49, Mar 3 1994.

[3] E. Ben-Jacob, I. Cohen, and D. L. Gutnick, "Cooperative organization of bacterial colonies: From genotype to morphotype," *Annual Review of Microbiology,* vol. 52, pp. 779-806, 1998.

[4] A. Be'er, H. P. Zhang, E. L. Florin, S. M. Payne, E. Ben-Jacob, and H. L. Swinney, "Deadly competition between sibling bacterial colonies," *Proceedings of the National Academy of Sciences of the United States of America,* vol. 106, no. 2, pp. 428-433, Jan 13 2009.

[5] A. Karimi, D. Karig, A. Kumar, and A. M. Ardekani, "Interplay of physical mechanisms and biofilm processes: review of microfluidic methods," *Lab on a Chip,* vol. 15, no. 1, pp. 23-42, 2015.

[6] D. Kaiser and R. Losick, "How and Why Bacteria Talk to Each Other," *Cell,* vol. 73, no. 5, pp. 873-885, Jun 4 1993.

[7] D. Kaiser, "Bacteria also vote," *Science,* vol. 272, no. 5268, pp. 1598-1599, Jun 14 1996.

[8] R. Wirth, A. Muscholl, and G. Wanner, "The role of pheromones in bacterial interactions," *Trends in Microbiology,* vol. 4, no. 3, pp. 96-103, Mar 1996.

[9] E. Ben Jacob, I. Becker, Y. Shapira, and H. Levine, "Bacterial linguistic communication and social intelligence," *Trends in Microbiology,* vol. 12, no. 8, pp. 366-372, Aug 2004.

[10] B. L. Bassler and R. Losick, "Bacterially speaking," *Cell,* vol. 125, no. 2, pp. 237-246, Apr 21 2006.

[11] S. B. von Bodman, J. M. Willey, and S. P. Diggle, "Cell-cell communication in bacteria: united we stand," *Journal of bacteriology,* vol. 190, no. 13, pp. 4377-4391, 2008.

[12] M. B. Miller and B. L. Bassler, "Quorum sensing in bacteria," *Annual Review of Microbiology,* vol. 55, pp. 165-199, 2001.

[13] C. M. Waters and B. L. Bassler, "Quorum sensing: Cell-to-cell communication in bacteria," *Annual Review of Cell and Developmental Biology,* vol. 21, pp. 319-346, 2005.

[14] K. Papenfort and B. L. Bassler, "Quorum sensing signal-response systems in Gram-negative bacteria," *Nature Reviews Microbiology,* vol. 14, no. 9, pp. 576-588, Sep 2016.

[15] R. De Dier, M. Fauvart, J. Michiels, and J. Vermant, "The role of biosurfactants in bacterial systems," in *The Physical Basis of Bacterial Quorum Communication*: Springer, 2015, pp. 189-204.

[16] D. López and R. Kolter, "Extracellular signals that define distinct and coexisting cell fates in Bacillus subtilis," *FEMS Microbiology Reviews,* vol. 34, no. 2, pp. 134-149, 2010/03/01 2010.

[17] E. Anne Shank and R. Kolter, "Extracellular signaling and multicellularity in Bacillus subtilis," *Current Opinion in Microbiology,* vol. 14, no. 6, pp. 741-747, 10/23 2011.

[18] R. F. Kinsinger, M. C. Shirk, and R. Fall, "Rapid surface motility in Bacillus subtilis is dependent on extracellular surfactin and potassium ion," *Journal of Bacteriology,* vol. 185, no. 18, pp. 5627-5631, Sep 2003.

[19] D. B. Kearns and R. Losick, "Swarming motility in undomesticated Bacillus subtilis," *Molecular Microbiology,* vol. 49, no. 3, pp. 581-590, Aug 2003.

[20] A. Venieraki, P. C. Tsalgatidou, D. G. Georgakopoulos, M. Dimou, and P. Katinakis, "Swarming motility in plant-associated bacteria," in *Hellenic Plant Protection Journal* vol. 9, ed, 2016, p. 16.

[21] G. Ariel, A. Rabani, S. Benisty, J. D. Partridge, R. M. Harshey, and A. Be'er, "Swarming bacteria migrate by Levy Walk," *Nature Communications,* vol. 6, Sep 2015.

[22] R. M. Harshey and J. D. Partridge, "Shelter in a Swarm," *Journal of Molecular Biology,* vol. 427, no. 23, pp. 3683-3694, Nov 20 2015.

[23] S. S. Branda, J. E. Gonzalez-Pastor, S. Ben-Yehuda, R. Losick, and R. Kolter, "Fruiting body formation by Bacillus subtilis," *Proceedings of the National Academy of Sciences of the United States of America,* vol. 98, no. 20, pp. 11621-11626, Sep 25 2001.

[24] A. Driks, "Overview: development in bacteria: spore formation in Bacillus subtilis," *Cellular and Molecular Life Sciences,* vol. 59, no. 3, pp. 389-391, Mar 2002.

[25] G. M. Dunny, T. J. Brickman, and M. Dworkin, "Multicellular behavior in bacteria: communication, cooperation, competition and cheating," *Bioessays,* vol. 30, no. 4, pp. 296-298, 2008.

[26] L. Chao and B. R. Levin, "Structured Habitats and the Evolution of Anticompetitor Toxins in Bacteria," *Proceedings of the National Academy of Sciences of the United States of America-Biological Sciences,* vol. 78, no. 10, pp. 6324-6328, 1981.

[27] V. C. Thomas and L. E. Hancock, "Suicide and fratricide in bacterial biofilms," *International Journal of Artificial Organs,* vol. 32, no. 9, pp. 537-544, Sep 2009.

[28] A. Be'er, S. Benisty, G. Ariel, and E. Ben-Jacob, "Interplay Between Sibling Bacterial Colonies," in *The Physical Basis of Bacterial Quorum Communication*, S. J. Hagen, Ed. New York, NY: Springer New York, 2015, pp. 145-162.

[29] K. A. Gibbs, M. L. Urbanowski, and E. P. Greenberg, "Genetic determinants of self identity and social recognition in bacteria," *Science,* vol. 321, no. 5886, pp. 256-259, Jul 11 2008.

[30] P. Stefanic, B. Kraigher, N. A. Lyons, R. Kolter, and I. Mandic-Mulec, "Kin discrimination between sympatric Bacillus subtilis isolates," *Proceedings of the National Academy of Sciences of the United States of America,* vol. 112, no. 45, pp. 14042-14047, Nov 10 2015.

[31] N. A. Lyons, B. Kraigher, P. Stefanic, I. Mandic-Mulec, and R. Kolter, "A Combinatorial Kin Discrimination System in Bacillus subtilis," *Current Biology,* vol. 26, no. 6, pp. 733-742, Mar 21 2016.

[32] B. Chakraborty, A. Mallick, S. Annagiri, S. Sengupta, and T. K. Sengupta, "Deciphering a survival strategy during the interspecific competition between Bacillus cereus MSM-S1 and Pseudomonas sp. MSM-M1," *R Soc Open Sci,* vol. 3, no. 11, p. 160438, Nov 2016.

[33] P. Patra, C. N. Vassallo, D. Wall, and O. A. Igoshin, "Mechanism of Kin-Discriminatory Demarcation Line Formation between Colonies of Swarming Bacteria," *Biophysical Journal,* vol. 113, no. 11, pp. 2477-2486, 2017/12/05/ 2017.

[34] H. Fujikawa and M. Matsushita, "Bacterial Fractal Growth in the Concentration Field of Nutrient," *Journal of the Physical Society of Japan,* vol. 60, no. 1, pp. 88-94, Jan 1991.

[35] J. Wakita, K. Komatsu, A. Nakahara, T. Matsuyama, and M. Matsushita, "Experimental Investigation on the Validity of Population-Dynamics Approach to Bacterial Colony Formation," *Journal of the Physical Society of Japan,* vol. 63, no. 3, pp. 1205-1211, Mar 1994.

[36] A. Seminara *et al.*, "Osmotic spreading of Bacillus subtilis biofilms driven by an extracellular matrix," *Proceedings of the National Academy of Sciences of the United States of America,* vol. 109, no. 4, pp. 1116-1121, Jan 24 2012.

[37] S. Trinschek, K. John, and U. Thiele, "From a thin film model for passive suspensions towards the description of osmotic biofilm spreading," *Aims Materials Science,* vol. 3, no. 3, pp. 1138-1159, 2016.

[38] J. Yan, C. D. Nadell, H. A. Stone, N. S. Wingreen, and B. L. Bassler, "Extracellular-matrix-mediated osmotic pressure drives Vibrio cholerae biofilm expansion and cheater exclusion," *Nature communications,* vol. 8, no. 1, p. 327, 2017.

[39] S. Trinschek, K. John, S. Lecuyer, and U. Thiele, "Continuous versus Arrested Spreading of Biofilms at Solid-Gas Interfaces: The Role of Surface Forces," *Physical Review Letters,* vol. 119, no. 7, Aug 16 2017.

[40] W. J. Ke, Y. H. Hsueh, Y. C. Cheng, C. C. Wu, and S. T. Liu, "Water surface tension modulates the swarming mechanics of Bacillus subtilis," *Frontiers in Microbiology,* vol. 6, Sep 24 2015.

[41] A. Be'er, R. S. Smith, H. P. Zhang, E. L. Florin, S. M. Payne, and H. L. Swinney, "Paenibacillus dendritiformis Bacterial Colony Growth Depends on Surfactant but Not on Bacterial Motion," *Journal of Bacteriology,* vol. 191, no. 18, pp. 5758-5764, Sep 15 2009.

[42] S. Trinschek, K. John, and U. Thiele, "Modelling of surfactant-driven front instabilities in spreading bacterial colonies," *Soft Matter,* vol. 14, no. 22, pp. 4464-4476, Jun 14 2018.

[43] A. Yang, W. S. Tang, T. Y. Si, and J. X. Tang, "Influence of Physical Effects on the Swarming Motility of Pseudomonas aeruginosa," *Biophysical Journal,* vol. 112, no. 7, pp. 1462-1471, Apr 11 2017.

[44] A. Be'er *et al.*, "Lethal protein produced in response to competition between sibling bacterial colonies," *Proceedings of the National Academy of Sciences of the United States of America,* vol. 107, no. 14, pp. 6258-6263, Apr 6 2010.

[45] A. Be'er, E. L. Florin, C. R. Fisher, H. L. Swinney, and S. M. Payne, "Surviving Bacterial Sibling Rivalry: Inducible and Reversible Phenotypic Switching in Paenibacillus dendritiformis," *Mbio,* vol. 2, no. 3, May-Jun 2011.

[46] A. Bridier, D. Le Coq, F. Dubois-Brissonnet, V. Thomas, S. Aymerich, and R. Briandet, "The Spatial Architecture of Bacillus subtilis Biofilms Deciphered Using a Surface-Associated Model and In Situ Imaging," *Plos One,* vol. 6, no. 1, Jan 18 2011.

[47] J. R. Porter, "Antony Van Leeuwenhoek - Tercentenary of His Discovery of Bacteria," *Bacteriological Reviews,* vol. 40, no. 2, pp. 260-269, 1976.

[48] S. Kojima and D. F. Blair, "The bacterial flagellar motor: Structure and function of a complex molecular machine," *International Review of Cytology - a Survey of Cell Biology, Vol. 233,* vol. 233, pp. 93-134, 2004.

[49] R. M. Macnab and S.-I. Aizawa, "Bacterial motility and the bacterial flagellar motor," *Annual review of biophysics and bioengineering,* vol. 13, no. 1, pp. 51-83, 1984.

[50] H. Terashima, S. Kojima, and M. Homma, "Flagellar motility in bacteria: structure and function of flagellar motor," *International review of cell and molecular biology,* vol. 270, pp. 39-85, 2008.

[51] J. Narayanan, J. Y. Xiong, and X. Y. Liu, "Determination of agarose gel pore size: Absorbance measurements vis a vis other techniques," *International Conference on Materials for Advanced Technologies (Icmat 2005),* vol. 28, pp. 83-+, 2006.

[52] S. i. Nishiyama, T. Umemura, T. Nara, M. Homma, and I. Kawagishi, "Conversion of a bacterial warm sensor to a cold sensor by methylation of a single residue in the presence of an attractant," *Molecular microbiology,* vol. 32, no. 2, pp. 357-365, 1999.

[53] R. M. Macnab and D. Koshland, "The gradient-sensing mechanism in bacterial chemotaxis," *Proceedings of the National Academy of Sciences,* vol. 69, no. 9, pp. 2509-2512, 1972.

[54] I. B. Zhulin, "A novel phototaxis receptor hidden in the cyanobacterial genome," *Journal of molecular microbiology and biotechnology,* vol. 2, no. 4, pp. 491-494, 2000.

[55] J. E. Gonzalez-Pastor, E. C. Hobbs, and R. Losick, "Cannibalism by sporulating bacteria," *Science,* vol. 301, no. 5632, pp. 510-513, Jul 25 2003.

[56] M. Fauvart *et al.*, "Surface tension gradient control of bacterial swarming in colonies of Pseudomonas aeruginosa," *Soft Matter,* vol. 8, no. 1, pp. 70-76, 2012.

[57] D. B. Kearns, "A field guide to bacterial swarming motility," *Nature Reviews Microbiology,* vol. 8, no. 9, pp. 634-644, Sep 2010.

[58] C. Giverso, M. Verani, and P. Ciarletta, "Emerging morphologies in round bacterial colonies: comparing volumetric versus chemotactic expansion," *Biomechanics and Modeling in Mechanobiology,* journal article vol. 15, no. 3, pp. 643-661, June 01 2016.

[59] K. H. Nealson, T. Platt, and J. W. Hastings, "Cellular control of the synthesis and activity of the bacterial luminescent system," *Journal of bacteriology,* vol. 104, no. 1, pp. 313-322, 1970.

[60] K. H. Nealson, "Autoinduction of bacterial luciferase," *Archives of microbiology,* vol. 112, no. 1, pp. 73-79, 1977.

[61] A. Eldar, "Social conflict drives the evolutionary divergence of quorum sensing," *Proceedings of the National Academy of Sciences of the United States of America,* vol. 108, no. 33, pp. 13635-13640, Aug 16 2011.

[62] N. B. Turan, D. S. Chormey, Ç. Büyükpınar, G. O. Engin, and S. Bakirdere, "Quorum sensing: Little talks for an effective bacterial coordination," *TrAC Trends in Analytical Chemistry,* vol. 91, pp. 1-11, 2017/06/01/ 2017.

[63] D. Wall, "Kin Recognition in Bacteria," *Annual Review of Microbiology,* vol. 70, no. 1, pp. 143-160, 2016/09/08 2016.

[64] J. A. Shapiro, "Thinking about bacterial populations as multicellular organisms," *Annual Review of Microbiology,* vol. 52, pp. 81-104, 1998.

[65] J. E. Strassmann, O. M. Gilbert, and D. C. Queller, "Kin Discrimination and Cooperation in Microbes," *Annual Review of Microbiology, Vol 65,* vol. 65, pp. 349-367, 2011.

[66] B. Mielich-Süss and D. Lopez, "Molecular mechanisms involved in Bacillus subtilis biofilm formation," *Environmental microbiology,* vol. 17, no. 3, pp. 555-565, 07/07 2015.

[67] P. W. Lindum, U. Anthoni, C. Christophersen, L. Eberl, S. Molin, and M. Givskov, "N-acyl-L-homoserine lactone autoinducers control production of an extracellular lipopeptide biosurfactant required for swarming motility of Serratia liquefaciens MG1," *Journal of Bacteriology,* vol. 180, no. 23, pp. 6384-6388, Dec 1998.

[68] J. P. Claverys and L. S. Havarstein, "Cannibalism and fratricide: mechanisms and raisons d'etre," *Nature Reviews Microbiology,* vol. 5, no. 3, pp. 219-229, Mar 2007.

[69] T. R. Malthus, *An essay on the principle of population: or, A view of its past and present effects on human happiness*. Reeves & Turner, 1888.

[70] K. E. Boulding, "The Malthusian Model As a General System," *Social and Economic Studies,* vol. 4, no. 3, pp. 195-205, 1955.

[71] M. Akhmet, H. Öktem, S. Pickl, and G. W. Weber, "An anticipatory extension of Malthusian model," in *AIP Conference Proceedings*, 2006, vol. 839, no. 1, pp. 260-264: AIP.

[72] C. Darwin, *On the origin of species*. Routledge, 1859.

[73] P.-F. Verhulst, "Notice sur la loi que la population suit dans son accroissement," *Corresp. Math. Phys.,* vol. 10, pp. 113-126, 1838.

[74] M. Peleg, M. G. Corradini, and M. D. Normand, "The logistic (Verhulst) model for sigmoid microbial growth curves revisited," *Food Research International,* vol. 40, no. 7, pp. 808-818, 2007.

[75] P. Schuster, "Mathematical modeling of evolution. Solved and open problems," *Theory in Biosciences,* vol. 130, no. 1, pp. 71-89, Mar 2011.

[76] J. Monod, "The Growth of Bacterial Cultures," *Annual Review of Microbiology,* vol. 3, pp. 371-394, 1949.

[77] J. A. Robinson and J. M. Tiedje, "Non-Linear Estimation of Monod Growth Kinetic-Parameters from a Single Substrate Depletion Curve," *Applied and Environmental Microbiology,* vol. 45, no. 5, pp. 1453-1458, 1983.

[78] C. Giverso, M. Verani, and P. Ciarletta, "Branching instability in expanding bacterial colonies," *Journal of The Royal Society Interface,* 10.1098/rsif.2014.1290 vol. 12, no. 104, 2015.

[79] C. Giverso, M. Verani, and P. Ciarletta, "Mechanically Driven Branching of Bacterial Colonies," *Journal of Biomechanical Engineering,* vol. 137, no. 7, p. 071003, 2015.

[80] E. Benjacob, O. Schochet, A. Tenenbaum, I. Cohen, A. Czirok, and T. Vicsek, "Generic Modeling of Cooperative Growth-Patterns in Bacterial Colonies," *Nature,* vol. 368, no. 6466, pp. 46-49, Mar 3 1994.

[81] S. K. Schmidt, S. Simkins, and M. Alexander, "Models for the kinetics of biodegradation of organic compounds not supporting growth," *Applied and Environmental Microbiology,* vol. 50, no. 2, p. 323, 1985.

[82] I. Golding, Y. Kozlovsky, I. Cohen, and E. Ben-Jacob, "Studies of bacterial branching growth using reaction-diffusion models for colonial development," *Physica a-Statistical Mechanics and Its Applications,* vol. 260, no. 3-4, pp. 510-554, Nov 15 1998.

[83] E. Benjacob, I. Cohen, O. Shochet, A. Tenenbaum, T. Vicsek, and A. Czirok, "Cooperative Formation of Chiral Patterns during Growth of Bacterial Colonies," *Physical Review Letters,* vol. 75, no. 15, pp. 2899-2902, Oct 9 1995.

[84] E. BenJacob, I. Cohen, A. Czirok, T. Vicsek, and D. L. Gutnick, "Chemomodulation of cellular movement, collective formation of vortices by swarming bacteria, and colonial development," *Physica a-Statistical Mechanics and Its Applications,* vol. 238, no. 1-4, pp. 181-197, Apr 15 1997.

[85] H. Hu and R. G. Larson, "Marangoni effect reverses coffee-ring depositions," *The Journal of Physical Chemistry B,* vol. 110, no. 14, pp. 7090-7094, 2006.

[86] E. Denamur and I. Matic, "Evolution of mutation rates in bacteria," *Molecular microbiology,* vol. 60, no. 4, pp. 820-827, 2006.

[87] M. B. H. Najafi and P. Pezeshki, "Bacterial mutation; types, mechanisms and mutant detection methods: a review," *European Scientific Journal, ESJ,* vol. 9, no. 10, 2014.

[88] J. N. Wilking, V. Zaburdaev, M. De Volder, R. Losick, M. P. Brenner, and D. A. Weitz, "Liquid transport facilitated by channels in Bacillus subtilis biofilms," *Proceedings of the National Academy of Sciences of the United States of America,* vol. 110, no. 3, pp. 848-852, Jan 15 2013.

[89] A. Valiei, A. Kumar, P. P. Mukherjee, Y. Liu, and T. Thundat, "A web of streamers: biofilm formation in a porous microfluidic device," *Lab on a Chip,* vol. 12, no. 24, pp. 5133-5137, 2012.

[90] A. Kumar *et al.*, "Microscale confinement features can affect biofilm formation," *Microfluidics and Nanofluidics,* vol. 14, no. 5, pp. 895-902, May 2013.

[91] H. S. Kotian *et al.*, "Spatial Awareness of a Bacterial Swarm," *bioRxiv,* 10.1101/341529 2018.

[92] N. Singh, V. Agrawal, S. C. Pemmaraju, R. Panwar, and V. Pruthi, "Impact of infectious Candida albicans biofilm on biomaterials," *Indian Journal of Biotechnology,* vol. 10, no. 4, pp. 417-422, Oct 2011.

[93] R. Iibuchi, Y. Hara-Kudo, A. Hasegawa, and S. Kumagai, "Survival of Salmonella on a Polypropylene Surface under Dry Conditions in Relation to Biofilm-Formation Capability," *Journal of Food Protection,* vol. 73, no. 8, pp. 1506-1510, Aug 2010.

Appendix

Benchmarking MATLAB® Codes

MATLAB® codes for the reaction diffusion equations used in this thesis have been benchmarked against analytical solution obtained from one dimensional diffusion equation for a semi-infinite domain.

Benchmarking Problem

$$\frac{\partial T}{\partial t} = D\frac{\partial^2 T}{\partial x^2} \tag{A.1}$$

Initial and Boundary Conditions

$$\begin{aligned} T\left(t=0,x\right) &= T_0 \\ T\left(t,x=0\right) &= T_1 \end{aligned} \tag{A.2}$$

The schematic in Figure A.1 shows the domain of simulation with the initial and boundary conditions.

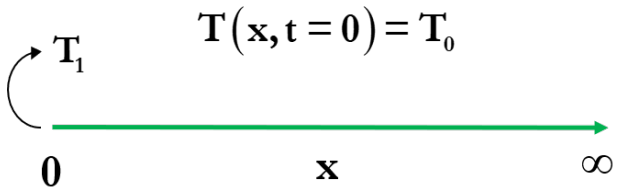

Fig. A.1. Domain for the benchmarking problem showing initial and boundary conditions

For the one dimensional diffusion equation (A.1), with initial and boundary conditions as prescribed by (A.2), the analytical solution is given by:

$$\frac{T-T_1}{T_0-T_1}=erf\left(\frac{x}{\sqrt{4Dt}}\right) \tag{A.3}$$

The parameters chosen for the benchmarking are as follows: $D=10^{-2}\ \mathrm{m^2/s}$, $T_0=1$ and $T_1=0$. The MATLAB® code for the two-colony model is modified and compared with the analytical solution as shown in Figure A.1. The analytical solution is found to match well with the analytical solution.

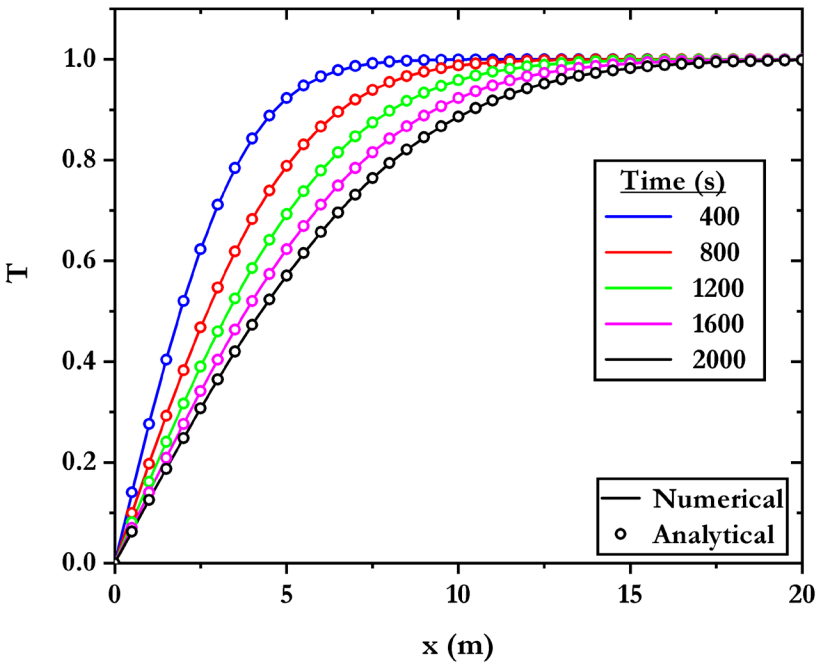

Fig. A.2. Benchmarking of numerical solution with analytical solution.

MATLAB® Codes

Solution of Single Colony Model

```
% % % % % % % % % % % % % % % % % % % % % % % % % % % % % % % % % % % % % % 
% This code calculates the numerical solution of the single-colony model. %
% Dimensional parameters  used  for  non-dimensionalization are: specific %
% growth rate r0 = 4/h, nutrient diffusion coefficient D_c = 1e-3 mm^2/h, %
% initial nutrient concentration c0 = 15 g/L, initial population  density %
% X0 = 1e-3, yield  gamma = 16 g/L, half saturation constant k = 42.5 g/L,%
% threshold nutrient concentration c* = 1.5 g/L, critical time  t* = 20h, %
% Domain size 2*R = 92 mm.  Dimensional simulation variables are: space x %
% and y, time t, population density X1, X2, X = X1 + X2, nutrient conc. c.%
% The  colony  diffusion  coefficient  D_b  is  estimated in terms of the %
% normalized diffusion coefficient D_bar = D_b/D_c.Simulation is performed%
% in the polar coordinate system. The single-colony model consisting of a %
% pair  of  coupled  ODEs is solved in terms of non-dimensional variables %
% using two nested loops.  The outer loop updates the time, the inner loop%
% corresponds to the r coordinate.  The  solution  for c_bar is evaluated %
% using an explicit scheme. For X_bar, an implicit scheme is used for the %
% solution, A*X=b where A is a square matrix and b is a column matrix.    %
% % % % % % % % % % % %  % %  % % % % % % % % % % % % % %  % % % %  % % % %

clear
close all
clc

%% Dimensional Parameters
r0=4;           % Specific growth rate
k=42.5;         % Half saturation constant
gamma=16;       % Yield
D_c=1e-3;       % Nutrient Diffusion coefficient
X_e=0.08;       % Population at Colony Edge
c0=15;          % Initial nutrient concentration
X0=1e-3;        % Initial Population density
R_p=46;         % Radius of Petri-dish
rho=2.5;        % Radius of drop cast

%% Dimensionless Parameters
D_bar=40;               % Normalized Diffusion coefficient
k_bar=k/c0;             % Half saturation constant
gamma_bar=gamma*X0/c0;  % Yield
alpha=0.1;              % Threshold Nutrient Concentration
X_e_bar=X_e/X0;         % Population at Colony Edge

%% Definition of Simulation Domain and Grid Generation

dr=1e-1;                % Dimensional grid size
dt=1e-3;                % Dimensional time step
r=0:dr:R_p;             % Dimensional Radial coordinate
t=0:1e-3:40;            % Dimensional Time

tau=t*r0;               % Dimensionless Time
r_bar=r*sqrt(r0/D_c);   % Dimensionless Radial coordinate
dtau=mean(diff(tau));   % Dimensionless time step
dr_bar=mean(diff(r_bar));% Dimensionless grid size

%% Initial conditions

% Dimensionless Nutrient concentration
c_bar=ones(size(r_bar));    % Initializing c_bar = 1
c_bar_n=c_bar;              % Updated nutrient conc.
```

```
X_bar=zeros(size(r_bar));    % Population density
A=zeros(length(r_bar));      % Coefficient matrix
b=zeros(length(r_bar),1);    % Column matrix
R=zeros(size(tau));          % Colony Radius

X_bar(1:rho/dr+1)=1;         % Initializing X_bar, X_bar = 1 inside drop cast
                             %                       = 0 elsewhere

A(1,1:2)=[1,-1];             % Boundary condition for X_bar
A(end,end-1:end)=[1,-1];     %


% Numerical Solution of Coupled ODEs
for nt=2:length(tau)    % Time loop

    % Solution of c_bar
    for i=2:length(r_bar)-1 % r_bar loop

        % Explicit scheme is used for c_bar
        c_bar_n(i)=c_bar(i+1)*(dtau/dr_bar^2+dtau/(2*r_bar(i)*dr_bar))...
            +c_bar(i)*(1-dtau*gamma_bar*X_bar(i)/(k_bar+c_bar(i))-2*dtau/dr_bar^2)...
            +c_bar(i-1)*(dtau/dr_bar^2-dtau/(2*r_bar(i)*dr_bar));
     end

    % Boundary condition for c_bar
    c_bar_n(1)=c_bar_n(2);

    % Solution of X_bar
    for i=2:length(r_bar)-1 % r_bar loop

        % Implicit scheme is used for X_bar
        D_bar=D_bar*(c_bar(i)>alpha);

        % Evaluating the coefficient matrix A
        A(i,i-1:i+1)=[D_bar*(-dtau/dr_bar^2+dtau/(2*r_bar(i)*dr_bar)),...
        1-dtau*c_bar(i)/(k_bar+c_bar(i))+2*dtau*D_bar/dr_bar^2,...
        D_bar*(-dtau/dr_bar^2-dtau/(2*r_bar(i)*dr_bar))];
    end

    % Evaluating column matrix b
    b(2:end-1)=X_bar(2:end-1)';


    X_bar=A\b;      % Solution of X_bar

    % Colony radius
    R(nt)=r(sum((X_bar-X_e_bar>0))+1); % Edge of the colony is defined

    % Updating solution at the end of each time step
    c_bar=c_bar_n;

end % End of Time loop

%% Plotting Results
plot(t, 2*R,'b-','LineWidth', 2.0);
xlabel('Time (hours)');
ylabel('Colony Diameter (mm)');
```

```
% % % % % % % % % % % % % % % % % % % % % % % % % % % % % % % % % % % % % %
% This code calculates the numerical solution of the two-colony model.The %
% dimensional parameters  used  for  non-dimensionalization are: specific %
% growth rate r0 = 4/h, nutrient diffusion coefficient D_c = 1e-3 mm^2/h, %
% initial nutrient concentration c0 = 15 g/L, initial population  density %
% X0 = 1e-3, mortality coefficient mu = 30/h, yield  gamma = 16 g/L, half %
% saturation constant k = 42.5 g/L, threshold nutrient concentration c* = %
% 1.5 g/L, critical time  t* = 20h, Domain size 2*R = 92 mm.  Dimensional %
% simulation variables are: space x and y, time t, population density X1, %
% X2, X = X1 + X2, nutrient concentration c.  The  range of dimensionless %
% parameters defining the phase space are: colony separation 12.5 mm < d <%
% 30 mm,  and  colony diffusion coefficient 0.04 < D_b < 0.3 (in mm^2/h). %
% Simulation is performed in  Cartesian coordinate system. The two-colony %
% model is solved using FTCS scheme using three nested loops.  The  outer %
% loop updates the time, the two inner loop correspond to x and y coordi- %
% nates. For each time step, the  solutions for X1_bar, X2_bar and c_bar  %
% are updated and boundary conditions are enforced.                       %
% % % % % % % % % % % %  % %  % % % % % % % % % % % % % %  % % % %  % % % %

clc;
close all;
clear;


%% Relevant Dimensional Parameters

d=10;                        % Separation between colonies (mm)

r0=4;                        % Specific Growth Rate, r0 (/h)
D_c=0.001;                   % Nutrient Diffusion Coefficient, D_c (mm^2/h)
X0=1e-3;                     % Initial Population density, X0
X_edge=0.3;                  % Reference Population denoting colony boundary
r_pet=46;                    % Domain size (mm)
R=2.5;                       % Radius of Drop Cast (mm)
T=30;                        % Observation (simulation) time (hours)

%% Dimensionless Parameters

D_bar=40;                    % Normalized Diffusion coefficient

gamma_bar=0.00107;           % Yield, gamma_bar=gamma*X0/c0
alpha=0.1;                   % Threshold nutrient concentration, alpha=c*/c0
k_bar=2.83;                  % Half saturation constant, k_bar=k/c0
mu_bar=1e-2;                 % Mortality coefficient, mu_bar=mu*X0/r0
tau0=80;                     % Critical time tau0=r0*(t*)
X_edge_bar=X_edge/X0;        % Reference Population denoting colony boundary

%% Definition of Simulation Domain and Grid Generation

% Dimensional variables
dx=0.25;                     % Grid resolution in x, dx
dy=dx;                       % Grid resolution in y, dy

x=-r_pet:dx:r_pet;           % Location of grid points in x direction
y=-r_pet:dy:r_pet;           % Location of grid points in y direction
n_c=r_pet/dx+1;              % Index location of the origin

nt=1+5e3;                    % Number of time steps
t=linspace(0,T,nt);          % Time points

% Dimensionless variables
```

```
x_bar=x*sqrt(r0/D_c);       % Location of grid points in x direction
y_bar=y*sqrt(r0/D_c);       % Location of grid points in y direction
dx_bar=mean(diff(x_bar));   % Grid resolution in x, dx_bar
dy_bar=mean(diff(y_bar));   % Grid resolution in y, dy_bar

tau=r0*t;                   % Time points, tau=t*r0
dtau=mean(diff(tau));       % Time step


%% Initial Conditions

% Initializing Nutrient concentration
c_bar=ones(length(x),length(y));        % Initial Nutrient concentration, c_bar = 1

% Initializing Population densities
X1_bar=zeros(length(x),length(y));      % Population density of colony 1, X1_bar
X2_bar=zeros(length(x),length(y));      % Population density of colony 2, X2_bar

for i=1:length(x)
    for j=1:length(y)

        % Initializing X1_bar
        if (x(i)-d/2)^2+y(j)^2<=R^2     % Equation of drop cast 1
            X1_bar(i,j)=1;              % X1_bar = 1 inside drop cast,
                                        %          0 elsewhere

        % Initializing X2_bar
        elseif (x(i)+d/2)^2+y(j)^2<=R^2 % Equation of drop cast 2
            X2_bar(i,j)=1;              % X1_bar = 1 inside drop cast,
                                        %          0 elsewhere
        end
    end
end


X1_bar_n=X1_bar;        % Updated X1_bar, X1_bar_n
X2_bar_n=X2_bar;        % Updated X2_bar, X2_bar_n
c_bar_n=c_bar;          % Updated c_bar, c_bar_n


X=X1_bar+X2_bar;        % Total Population density


%% Numerical Solution

for n=1:nt                      % Time loop
    for i=2:length(x)-1         % x loop
        for j=2:length(y)-1     % y loop

            % Solution for X1_bar
            X1_bar_n(i,j)=D_bar*(c_bar(i,j)>=alpha)*dtau/dx_bar^2*...
                (X1_bar(i+1,j)+X1_bar(i-1,j))+...
             D_bar*(c_bar(i,j)>=alpha)*dtau/dy_bar^2*...
                (X1_bar(i,j+1)+X1_bar(i,j-1))+(1-(2*dtau*D_bar/dx_bar^2 ...
               +2*dtau*D_bar/dy_bar^2)*(c_bar(i,j)>=alpha)+dtau*c_bar(i,j)/...
               (c_bar(i,j)+k_bar))*X1_bar(i,j)-dtau*mu_bar*X1_bar(i,j)...
               *X2_bar(i,j)*(tau(n)>r0*20)*(X(n_c,n_c)<=X_edge/X0);

            % Solution for X2_bar
            X2_bar_n(i,j)=D_bar*(c_bar(i,j)>=alpha)*dtau/dx_bar^2*...
                (X2_bar(i+1,j)+X2_bar(i-1,j))+...
                D_bar*(c_bar(i,j)>=alpha)*dtau/dy_bar^2*...
```

```
                (X2_bar(i,j+1)+X2_bar(i,j-1))+(1-(2*dtau*D_bar/dx_bar^2 ...
                +2*dtau*D_bar/dy_bar^2)*(c_bar(i,j)>=alpha)+dtau*c_bar(i,j)/...
                (c_bar(i,j)+k_bar))*X2_bar(i,j)-dtau*mu_bar*X2_bar(i,j)...
                *X1_bar(i,j)*(tau(n)>r0*20)*(X(n_c,n_c)<=X_edge/X0);

            % Solution for c_bar
            c_bar_n(i,j)=dtau/dx_bar^2*(c_bar(i+1,j)+c_bar(i-1,j))...
                +dtau/dy_bar^2*(c_bar(i,j+1)+c_bar(i,j-1))+(1-2*dtau/dx_bar^2 ...
                -2*dtau/dy_bar^2-gamma_bar*dtau*(X1_bar(i,j)+X2_bar(i,j))...
                /(c_bar(i,j)+k_bar))*c_bar(i,j);
        end
    end

    % Enforcing Boundary Conditions
    X1_bar_n(1,:)=X1_bar_n(2,:);
    X2_bar_n(1,:)=X2_bar_n(2,:);
    X1_bar_n(end,:)=X1_bar_n(end-1,:);
    X2_bar_n(end,:)=X2_bar_n(end-1,:);
    X1_bar_n(:,1)=X1_bar_n(:,2);
    X2_bar_n(:,1)=X2_bar_n(:,2);
    X1_bar_n(:,end)=X1_bar_n(:,end-1);
    X2_bar_n(:,end)=X2_bar_n(:,end-1);

    % Solutions are updated at the end of each time step
    X1_bar=X1_bar_n;
    X2_bar=X2_bar_n;
    c_bar=c_bar_n;
    X=X1_bar+X2_bar;

    % Generating Contour Plot of Numerical Solution of X
    if mod(n,1000)==1   % Solution is plotted every 1000th time step
    contourf(x,y,X'*X0,100,'LineColor','none','LevelList',[0 X_edge]);
    title(['t = ',num2str((n-1)*dtau/r0),' h']);
    xlabel ('x (mm)')
    ylabel ('y (mm)')
    axis equal;
    colormap 'jet';
    colorbar;
    caxis([0 0.5]);
    drawnow();
    end

end  % End of time loop
```

Dimensionless Phase Diagram Generation

```
% % % % % % % % % % % % % % % % % % % % % % % % % % % % % % % % % % % % % %
% This code calculates the critical separation demarcating the coalescence%
% and interface phases in the phase-space consisting of the dimensionless %
% separation (d_bar) and  normalized  diffusion  coeffcient (D_bar).  All %
% parameters described in this code are in their dimensionless forms. The %
% dimensional parameters  used  for  non-dimensionalization are: specific %
% growth rate r0 = 4/h, nutrient diffusion coefficient D_c = 1e-3 mm^2/h, %
% initial nutrient concentration c0 = 15 g/L, initial population  density %
% X0 = 1e-3, mortality coefficient mu = 30/h, yield  gamma = 16 g/L, half %
% saturation constant k = 42.5 g/L, threshold nutrient concentration c* = %
% 1.5 g/L, critical time  t* = 20h, Domain size 2*R = 92 mm.  Dimensional %
% simulation variables are: space x and y, time t, population density X1, %
% X2, X = X1 + X2, nutrient concentration c.  The  range of dimensionless %
% parameters defining the phase space are: colony separation 12.5 mm < d <%
% 30 mm,  and  colony diffusion coefficient 0.04 < D_b < 0.3 (in mm^2/h). %
% Simulation is performed in  Cartesian coordinate system.                %
% % % % % % % % % % % % % % % % % % % % % % % % % % % % % % % % % % % % % %

clc;
close all;
clear;

%% Dimensionless Parameters

gamma_bar=0.00107;           % Yield, gamma_bar=gamma*X0/c0
alpha=0.1;                   % Threshold nutrient concentration, alpha=c*/c0
k_bar=2.83;                  % Half saturation constant, k_bar=k/c0
mu_bar=1e-2;                 % Mortality coefficient, mu_bar=mu*X0/r0
tau0=80;                     % Critical time tau0=r0*(t*)
X_edge_bar=3e2;              % Reference Population denoting colony boundary

%% Definition of Simulation Domain and Grid Generation

R_bar=3000;                  % Domain size 2R_bar x 2R_bar, R_bar= R*sqrt(r0/D_c)
r_bar=158;                   % Radius of drop cast, r=R*sqrt(r0/D_c)

dx_bar=25;                   % Grid resolution in x, dx_bar
dy_bar=dx_bar;               % Grid resolution in y, dy_bar

x_bar=-R_bar:dx_bar:R_bar;   % Location of grid points in x direction
y_bar=-R_bar:dy_bar:R_bar;   % Location of grid points in y direction
n_c=R_bar/dx_bar+1;          % Index location of the origin

dtau=1e-1;                   % Time step dtau
tau=0:dtau:100;               % Time points, tau=t*r0

%% Phase space Description

D_bar=40:10:300;             % Normalized Diffusion coefficient, D_bar=D_b/D_c
d_bar=700:dx_bar:3000;       % Colony separation d_bar=d*sqrt(r0/D_c)


%% Numerical Solution

% % % % % % % % % % % % % % % % % % % % % % % % % % % % % % % % % % % % % % %
% Solution Algorithm: The critical separation d_star is determined for each %
% value of D_bar within the chosen range. To do this, the two-colony model  %
% is solved within two nested loops corresponding to the phase variables.   %
% The outer loop successively increases D_bar,  while   the   inner   loop  %
% increases  d_bar. For each solution within the inner loop,    a check is  %
% performed which checks if the colonies separate. The value of d_bar for   %
```

```
% which two colonies start  forming  interface  is the critical separation  %
% d_star.   By running through the outer loop,   we obtain a set of d_star  %
% within the chosen range of D_bar.                                          %
% % % % % % % % % % % % % % % % % % % % % % % % % % % % % % % % % % % % % % %

d_star=zeros(1,length(D_bar));  % Critical separation, d_star

for l=1:length(D_bar)           % Outer loop: Increases D_bar


for k=1:length(d_bar)           % Inner loop: Increases d_bar

% Initial conditions

% Initializing Nutrient concentration
c_bar=ones(length(x_bar),length(y_bar));   % Initial Nutrient concentration, c_bar = 1

% Initializing Population densities

X1_bar=zeros(length(x_bar),length(y_bar));  % Population density of colony 1, X1_bar
X2_bar=zeros(length(x_bar),length(y_bar));  % Population density of colony 2, X2_bar

for i=1:length(x_bar)
    for j=1:length(y_bar)

        % Initializing X1_bar

        if (x_bar(i)-d_bar(k)/2)^2+y_bar(j)^2<=r_bar^2      % Equation of drop cast 1

            X1_bar(i,j)=1;                  % X1_bar = 1 inside drop cast,
                                            %          0 elsewhere


        % Initializing X2_bar

        elseif (x_bar(i)+d_bar(k)/2)^2+y_bar(j)^2<=r_bar^2  % Equation fo drop cast 2

            X2_bar(i,j)=1;                  % X2_bar = 1 inside drop cast,
                                            %          0 elsewhere
        end
    end
end

% Solution of Two-Colony Model

% % % % % % % % % % %  % %  % % % % % % % % % % % % % % % % %  % % % %  % % % % %
% The two-colony model is solved using FTCS scheme using three nested loops %
% The outer loop updates the time, the two inner loop correspond to x and y %
% coordinates. For each time step,   the  solutions for X1_bar, X2_bar and  %
% c_bar are updated and boundary conditions are enforced.                    %
% % % % % % % % % % %  % %  % % % % % % % % % % % % % % % % %  % % % %  % % % % %

X1_bar_n=X1_bar;      % Updated X1_bar, X1_bar_n
X2_bar_n=X2_bar;      % Updated X2_bar, X2_bar_n
c_bar_n=c_bar;        % Updated c_bar, c_bar_n
X=X1_bar+X2_bar;

for n=1:length(tau)                     % Time Loop
    for i=2:length(x_bar)-1             % x loop
        for j=2:length(y_bar)-1         % y loop

            % Solution for X1_bar
            X1_bar_n(i,j)=D_bar(l)*(c_bar(i,j)>=alpha)*dtau/dx_bar^2*...
```

```
                (X1_bar(i+1,j)+X1_bar(i-1,j))+...
                D_bar(l)*(c_bar(i,j)>=alpha)*dtau/dy_bar^2*...
                (X1_bar(i,j+1)+X1_bar(i,j-1))+(1-(2*dtau*D_bar(l)/dx_bar^2 ...
                +2*dtau*D_bar(l)/dy_bar^2)*(c_bar(i,j)>=alpha)+dtau*c_bar(i,j)/...
                (c_bar(i,j)+k_bar))*X1_bar(i,j)-dtau*mu_bar*X1_bar(i,j)...

*X2_bar(i,j)*(tau(n)>tau0)*(X1_bar(n_c,n_c)+X2_bar(n_c,n_c)<=X_edge_bar);

            % Solution for X2_bar
            X2_bar_n(i,j)=D_bar(l)*(c_bar(i,j)>=alpha)*dtau/dx_bar^2*...
                (X2_bar(i+1,j)+X2_bar(i-1,j))+...
                D_bar(l)*(c_bar(i,j)>=alpha)*dtau/dy_bar^2*...
                (X2_bar(i,j+1)+X2_bar(i,j-1))+(1-(2*dtau*D_bar(l)/dx_bar^2 ...
                +2*dtau*D_bar(l)/dy_bar^2)*(c_bar(i,j)>=alpha)+dtau*c_bar(i,j)/...
                (c_bar(i,j)+k_bar))*X2_bar(i,j)-dtau*mu_bar*X2_bar(i,j)...

*X1_bar(i,j)*(tau(n)>tau0)*(X1_bar(n_c,n_c)+X2_bar(n_c,n_c)<=X_edge_bar);

            % Solution for c_bar
            c_bar_n(i,j)=dtau/dx_bar^2*(c_bar(i+1,j)+c_bar(i-1,j))...
                +dtau/dy_bar^2*(c_bar(i,j+1)+c_bar(i,j-1))+(1-2*dtau/dx_bar^2 ...
                -2*dtau/dy_bar^2-gamma_bar*dtau*(X1_bar(i,j)+X2_bar(i,j))...
                /(c_bar(i,j)+k_bar))*c_bar(i,j);
        end
    end

    % Enforcing Boundary Conditions
    X1_bar_n(1,:)=X1_bar_n(2,:);
    X2_bar_n(1,:)=X2_bar_n(2,:);
    X1_bar_n(end,:)=X1_bar_n(end-1,:);
    X2_bar_n(end,:)=X2_bar_n(end-1,:);
    X1_bar_n(:,1)=X1_bar_n(:,2);
    X2_bar_n(:,1)=X2_bar_n(:,2);
    X1_bar_n(:,end)=X1_bar_n(:,end-1);
    X2_bar_n(:,end)=X2_bar_n(:,end-1);

    % Solutions are updated at the end of each time step
    X1_bar=X1_bar_n;
    X2_bar=X2_bar_n;
    c_bar=c_bar_n;
    X=X1_bar+X2_bar;

end  % End of Two-Colony Model solution


% Check for Interface formation for every d_bar

if X(n_c,n_c)<X_edge_bar    % If net population density at origin is less than
    d_star(l)=d_bar(k);     % X_edge_bar, an interface is formed.
    break;
end

end   % End of d_bar loop

% Dynamic Plotting of Phase Diagram

semilogx(D_bar(1:l),d_star(1:l),'b-','LineWidth',2.0);
xlabel ('$\mathbf{\bar{D}}$','Interpreter','latex');
ylabel ('d*');
axis([30 400 500 1700]);
drawnow();

end   % End of D_bar loop
```

Data Processing from Single Colony Experiments: Effective Colony Diameter

Main function

```
% % % % % % % % % % % %  % %  % % % % % % % % % % % % % % % % % % % % % % % %
% This code estimates the effective diameter of a single bacterial colony %
% at a given time point. The code inputs image collected from experiment. %
% From the input image file, a length scale is first established using the%
% im_scale function. Next, the code  isolates  the colony from background %
% using the crop function and computes  the  number   of  pixels that the %
% colony covers. This is then converted into the effective diameter using %
% the length scale computed earlier.                                      %
% % % % % % % % % % % %  % %  % % % % % % % % % % % % % % % % % % % % % % % %

clear;
close all;
clc;

%% Read image

% Navigate to folder containing saved image
current_folder=pwd;

cd ../../../'Experiments Rajorshi'/'B. subtilis radius rate experiments'/'0.5%
Repeat'/
im_folder=pwd;

% Select required image
im_name='Set 2.2 22 hours.JPG';

% Read image file into MATLAB
image=imread(im_name);

cd(current_folder);

%% Length Scale Estimation

scale=im_scale(image);           % im_scale outputs the length scale in terms of
                                 % size of pixel (mm/px)

%% Isolate colony

[~, colony]=crop(image);    % crop function returns binary image of isolated colony

subplot(2,1,1),imshow(colony);  % Comparison of original and colony-isolated
subplot(2,1,2),imshow(image);   % images.

%% Colony Diameter Estimate

colony_diameter=sqrt(sum(sum(colony)))*scale*sqrt(4/pi);
```

im_scale function

```
function scale=im_scale(image)

% % % % % % % % % % % % % % % % % % % % % % % % % % % % % % % % % % % % % % %
% The function inputs an image file. It displays the  image  and asks the %
% user to select two reference points on the image.  The length scale  is %
% computed based on the coordinates of the chosen reference points and  a %
% known length from the image.                                            %
% % % % % % % % % % % % % % % % % % % % % % % % % % % % % % % % % % % % % % %

% Step 1: Display image
imshow(image);

% Step 2: Ask user for two reference points
[x,y]=ginput(2);
px_dist=diff(y);

% Step 3: Prompt for entering a known length scale
length=input('Enter length in mm: ');

% Step 4: Determine the length scale in mm/px
scale=length/px_dist;

end
```

crop function

```
function [center,image_crop]=crop(image)

% % % % % % % % % % % % % % % % % % % % % % % % % % % % % % % % % % % % % % %
% The function inputs the RGB image of the colony and outputs the location%
% of the center of the colony and a binary image of the isolated  colony. %
% For isolating the colony, first, a mask is created around the colony by %
% picking points around the colony.  The  mask is then translated on to a %
% binary canvas.                                                          %
% % % % % % % % % % % % % % % % % % % % % % % % % % % % % % % % % % % % % % %

% Create mask around colony for isolating colony
imshow(image);
[x,y]=ginput;
center(1)=x(1);
center(2)=y(1);
x=[x; x(2)];
y=[y;y(2)];

crop_mask=poly2mask(x,y,size(image,1),size(image,2)); % Masked colony

% Generating binary image of isolated colony
image_bw=im2bw(image,0.58);
image_crop=(1-image_bw).*crop_mask;

end
```